Figure 17: TDS concentrations during 1600-gpm post-acid treatment aquifer test.

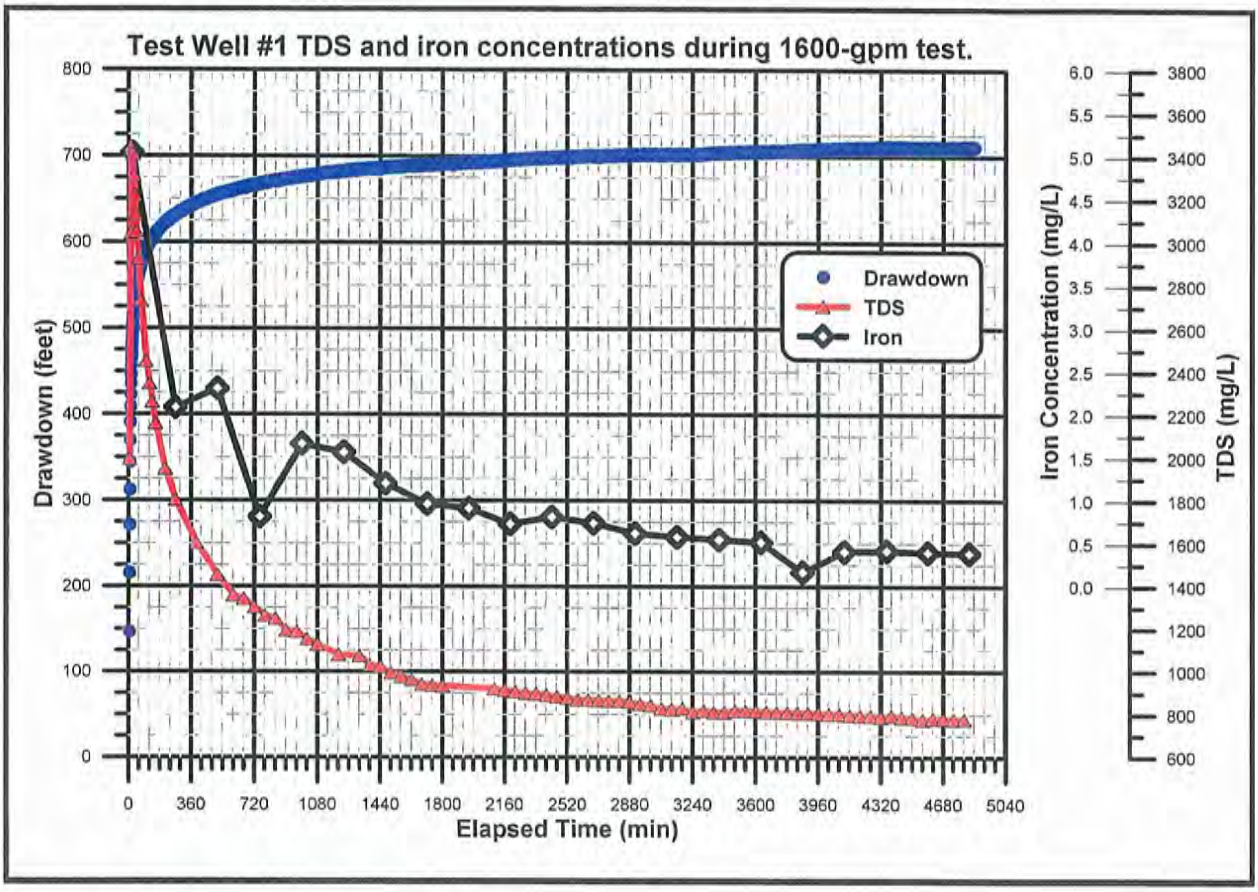

5 YIELD AND DRAWDOWN TESTS

Test Well #1 was subjected to a pre-frac stepped rate test on 3/10/2013 and tested at 500, 650, 800 and 950 gpm. The 950-gpm step could not be sustained due to the limitations of the test pump and decreased to 878 gpm before that step was terminated after 23 minutes, as compared to 120 minutes per step for the other rates. A 900-gpm constant rate test was conducted for 12 hours on 3/11/2013 to provide additional information about aquifer response.

It was evident from the March 2013 stepped rate and constant rate tests that the well did not satisfy the design target of a 1400-gpm production well and, therefore, it was necessary to stimulate the well production with high-pressure acid-frac treatment. Stimulation of the well with high-pressure hydraulic fracturing with acid was accomplished on 3/26/3013.

After the high-pressure acid frac treatment, the well was subjected to a post-frac stepped rate test on 4/13/2013. The step test consisted of five pumping rates, each of 2-hour duration, at 1015, 1115, 1210, 1310 and 1410 gpm. The stepped rate test was followed by an 81-hour constant rate test at 1600 gpm.

5.1 Barometric Response

Pre-test monitoring was accomplished for the purposes of (1) identifying any pre-test trend in groundwater levels and (2) to determine the effect of barometric pressure fluctuations on groundwater levels in the two wells used for the tests. The two wells were the pumped well, Test Well #1, and an observation well, Test Well #2A. Pre-test monitoring did not detect a significant trend in groundwater levels that would require application of a correction for the duration of the pumping tests.

Pre-test atmospheric barometric pressure and water level data were collected simultaneously for 52 hours and 12 minutes from 3/7/2013 at 9:48 A.M. through 3/9/2013 at 2:00 P.M., during which time barometric pressure fluctuated less than 0.25 inches Hg. Figure 18 shows changes in groundwater levels plotted versus changes in barometric pressure.

Figure 18: Pre-test static water level change versus barometric pressure change.

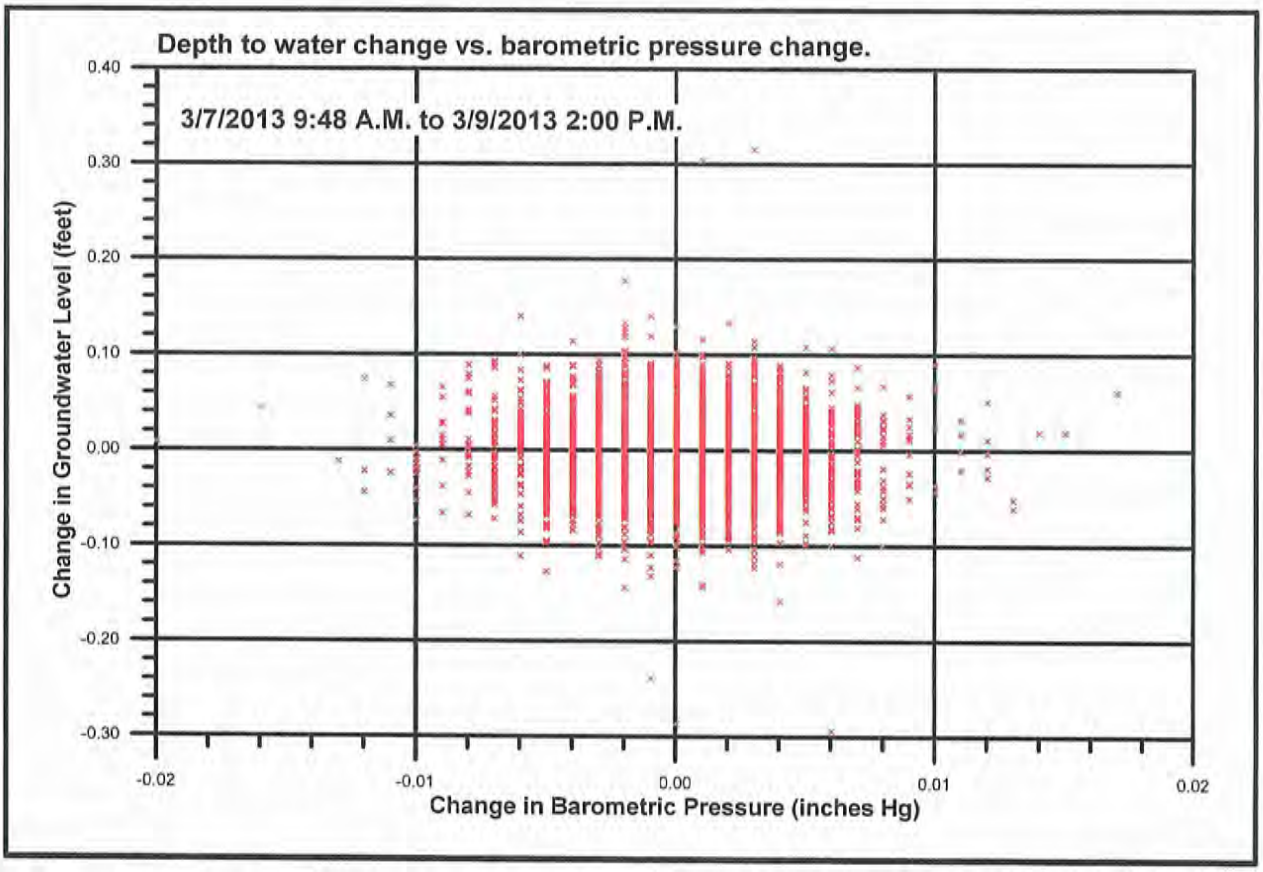

Figure 18 indicates that while barometric pressure is relatively stable, groundwater fluctuations are small and, in part, potentially reflect error inherent in the 500-psi pressure transducer used to measure groundwater levels. The pressure transducer is accurate to ±0.1% full scale, thus the fluctuation in the groundwater levels on Figure 18

might be explained as scatter in the instrument readings within the accuracy of the instrument. However, other ways of examining the data suggest something other than simple instrumentation data scatter has affected the data. Figure 19 shows the same data plotted as cumulative change in groundwater elevation versus cumulative change in barometric pressure.

Figure 19: Change in groundwater versus change in barometric pressure.

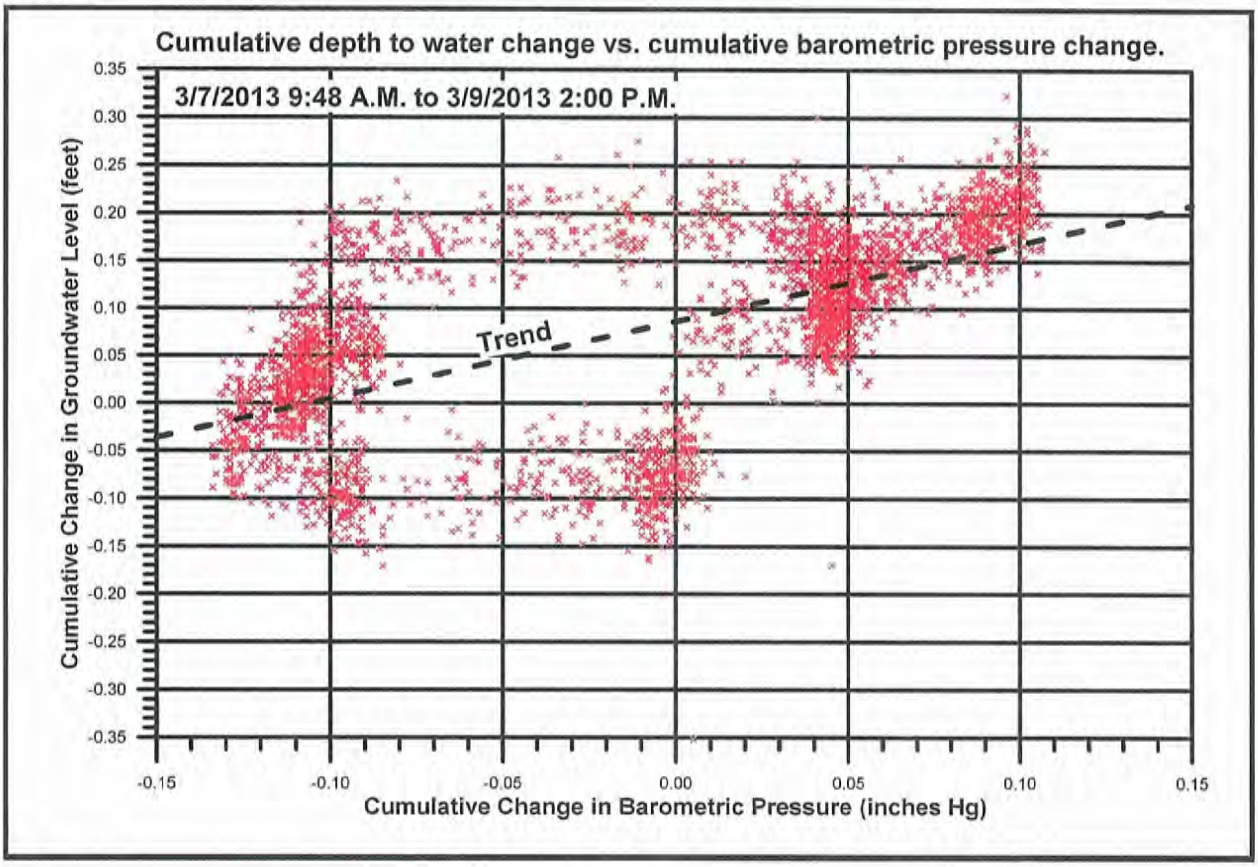

The data on Figure 19 describe an ellipsoid which represents a completed cycle in barometric pressure fluctuation with pressure departing from a starting value, rising or falling over a range of values and returning to the starting value. The ellipsoidal distribution of groundwater level fluctuation with respect to a cyclic fluctuation in barometric pressure is typical of confined groundwater response and the general orientation of the ellipsoid, as shown by the trend line on Figure 19, is generally representative of the response of the groundwater levels with respect to barometric pressure fluctuation during the barometric pressure fluctuation cycle.

It is anticipated that other small fluctuations in barometric pressure, less than a few tenths of an inch of mercury, will produce similar barometric pressure/groundwater level responses, including the ellipsoidal pattern. The most significant aspect of the barometric response on Figure 19 is that the groundwater level fluctuation in response

to small changes in barometric pressure is negligible compared to typical aquifer responses generated during the yield and drawdown testing of the aquifer. This conclusion is supported by the data plotted on Figure 20 where it is clear that significant changes in groundwater levels are a response to pumping whereas response to barometric fluctuation is too small to affect test interpretation. Accordingly, the data show there is no need to correct the pumping test data for aquifer barometric response.

Figure 20: Barometric fluctuations compared to groundwater levels.

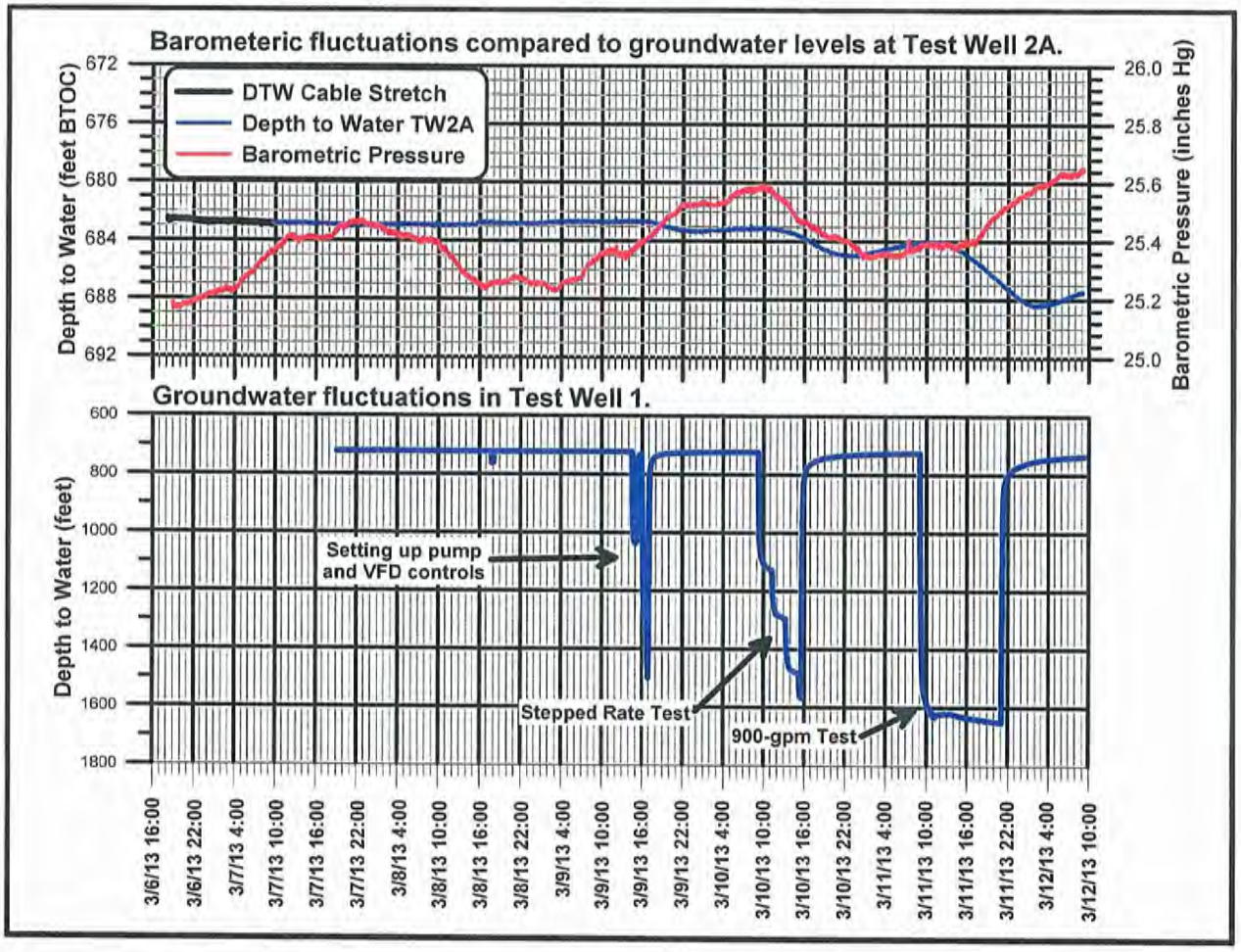

The latter conclusion is reinforced by data collected at Test Well #2A during the earlier testing of that well. The relationship between barometric pressure change and static water level fluctuation is shown on Figure 21, where a barometric change of approximately 0.30 inches mercury causes approximately 0.55 feet of groundwater level fluctuation.

Figure 21: Static water level and barometric fluctuation compared to Seattle tide.

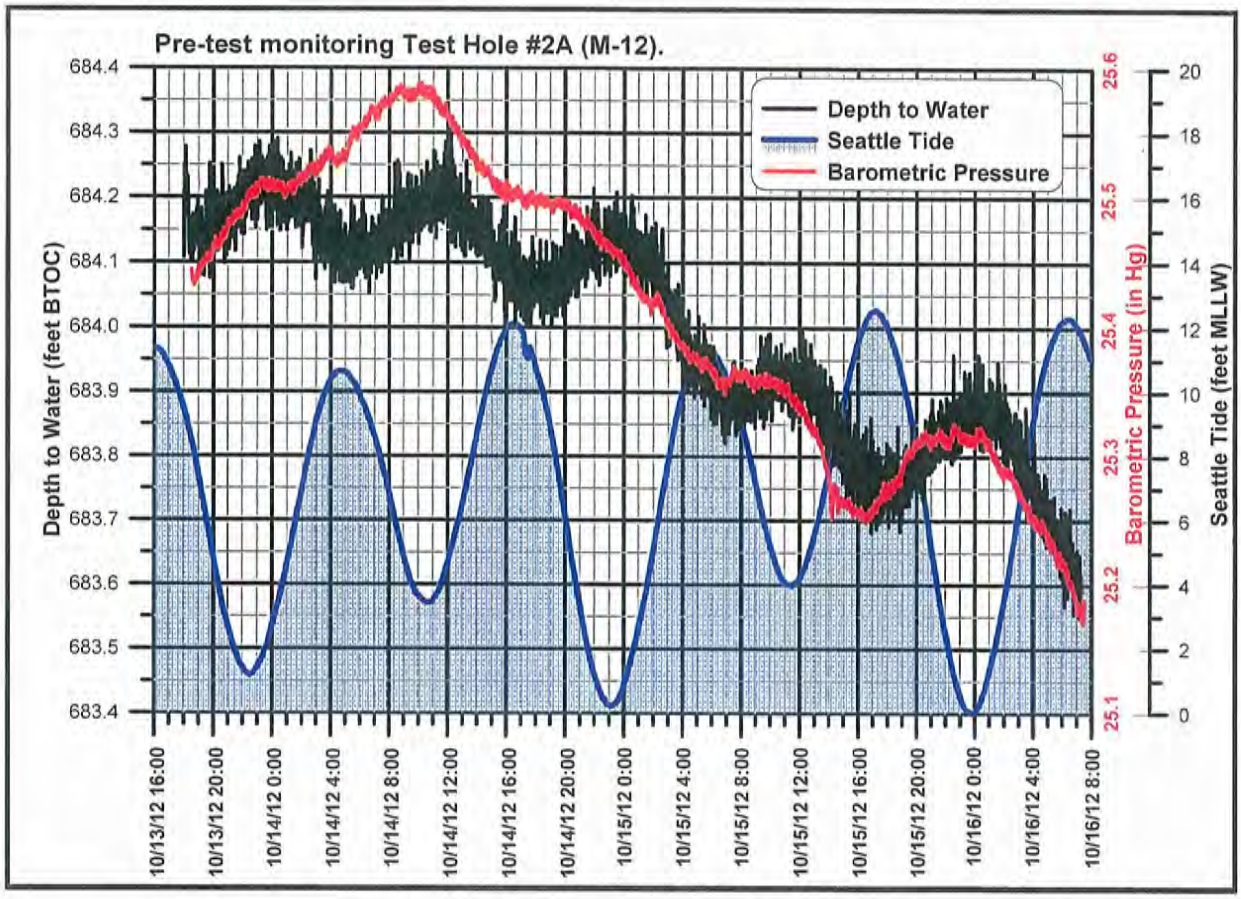

Figure 21 reflects the fact that when barometric pressure is relatively constant or fluctuating within a relatively narrow range, there is little fluctuation in the groundwater level. This is evident as a cluster of data on the right-hand side of the plot on Figure 22, for the period from 6:00 P.M. on 10/13/2012 through 4:00 P.M. on 10/14/2012 from Figure 21.

The remainder of the data correspond to the part of Figure 21 after 4:00 P.M., 10/14/2012, and describe a good relationship between the barometric pressure change and a corresponding and resulting change in the static water level in the aquifer, which is quantified by a linear regression line as shown on Figure 22.

Figure 22 exhibits significant data scatter around the linear regression line, similar to the data scatter evident in the cluster of data to the right of the linear regression line trend. The data associated with the linear regression hint at a cyclical nature to the scatter, similar to that observed on Figure 19. One source of the elliptical distribution of data on Figure 19 is suggested by Figure 21 which shows the static water level and barometric pressure data compared to the tide at Seattle, Washington, with the tidal data adjusted to plot in the exact time zone at Test Well #1 by correcting the tide time by the degrees, minutes and seconds of longitude between the Seattle tide recorder the test well. It is

evident from Figure 21 that earth tide at the test well causes a diurnal fluctuation of approximately 0.2 feet superimposed over the groundwater level observed in Test Well #1.

Figure 22: Change in static water level versus change in barometric pressure.

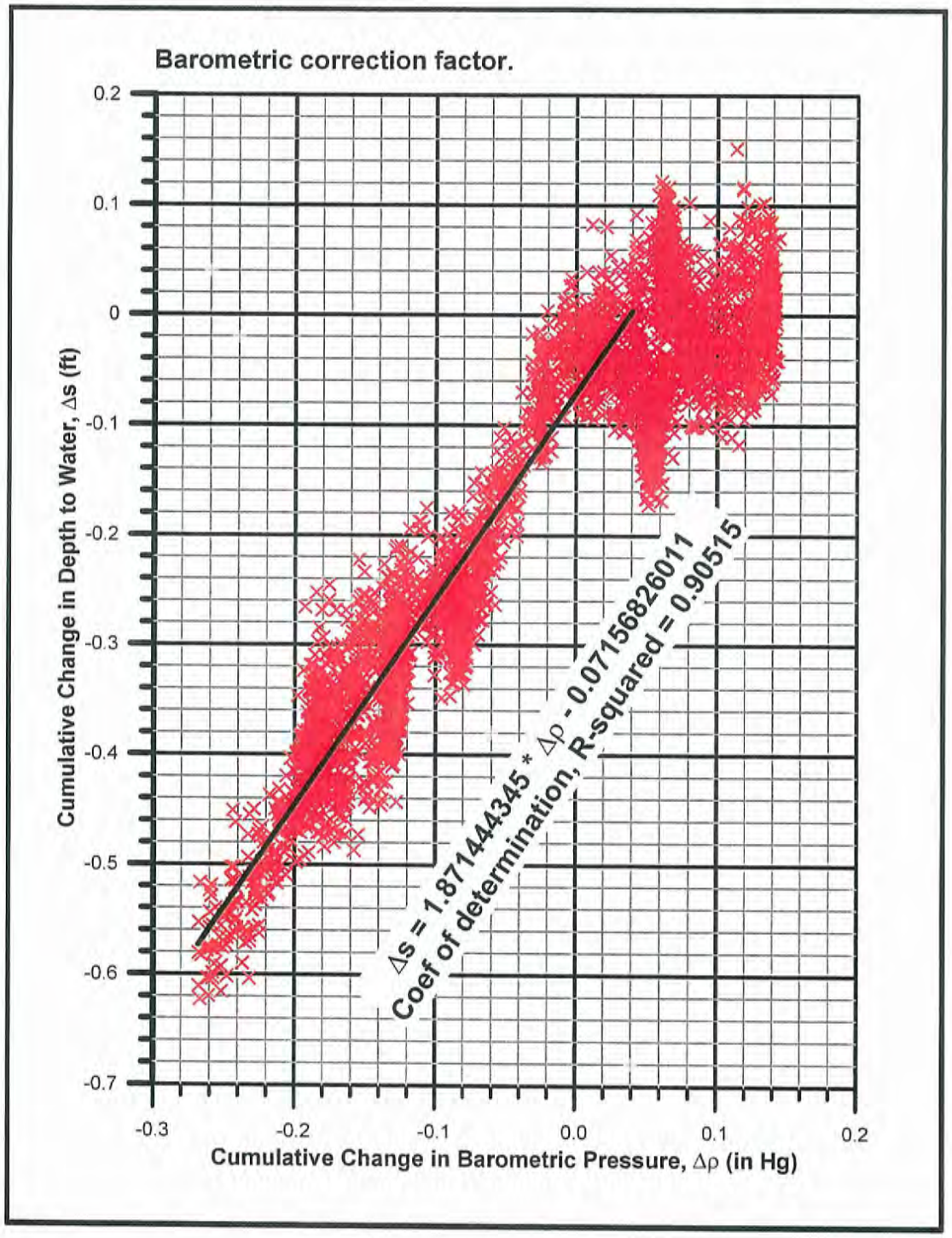

The diurnal fluctuation of approximately 0.2 feet is consistent with the width of the data scatter on each side of the linear regression line on Figure 22 and is the likely explanation for most of the data scatter on Figures 19 and 22. The fluctuation of the static water level approximately 0.55 feet in response to barometric pressure change combined with a 0.2-foot diurnal fluctuation due to earth tide, as shown on Figure 21, is insignificant with respect to the drawdown of the aquifer water level during pumping and is therefore not of concern in interpretation of time-drawdown data collected during pumping tests with pressure transducer equipment that is vented to eliminate barometric effects on the instrument.

5.2 Test Pump Equipment

Two test pumps were used during yield and drawdown testing of Test Well #1. Initially, a General Electric ESP EN35000 GE pump was installed. The latter pump was used for a 3/10/2013 stepped rate test, at rates ranging from 500 to 950 gpm, and a 3/11/2013 constant rate test at 900 gpm, prior to stimulation of the well with an acid frac treatment.

After stimulation of the well with acid frac treatment, the same pump was used for a 4/13/2013 stepped rate test of the well at rates ranging from 1015 to 1605 gpm. The VFD during the latter test was pre-set to ramp the pumping rate back if the current draw on the motors exceeded 150.9 amps. Part of the way through the 1605-gpm step, the 150.9-amp limit was exceeded and the VFD ramped the pumping rate back to 1475 gpm, thus terminating the step test. After review of the VFD output records, it was decided to operate the two submersible motors at 1100 hp or 110% by increasing the amperage limit to 164 amps for a 3-day test at 1600 gpm. When the pump was started to repeat the stepped rate test, the pump failed. When the failed pump was removed, it was found that more than 700 feet of electronic water level indicator wire that had been broken off in a standpipe by one of the Layne crew had fallen out of the standpipe and been ingested by the pump as shown in Photos 44 and 45.

The 12-stage ESP EN35000 GE pump was replaced by an 8-stage ESP TP1700 GE pump which had failed during the October 2012 stepped rate test of the well at Test Site #2A. The failure was determined to be the result of damage to the lower pump bowl during installation of the pressure jacket on the pump during its assembly. The pump was repaired while Test Well #1 was subjected to acid stimulation treatment and the pump was returned to service for the post-stimulation stepped rate and constant rate tests of Test Well #1.

5.2.1 ESP TN35000 12-Stage Pump

The pump inlet of the ESP TN35000 pump used in March 2013 was set at a depth of 1780.66 feet BGL in the 16-inch casing. The bottom of the pump motor was at a depth of 1864.47 feet BGL, 64.5 feet below the top of the 10-3/4 well casing which top is at 1800 feet. The static water level on 3/10/2013 was 724.8 feet below the top of the standpipes installed for the test. The tops of the standpipes were 1.917 feet AGL; therefore, the static water level was 722.9 feet BGL, providing pump inlet submergence at static of 1057.8 feet. Figures 23 and 24 provide pump performance curves.

Photo 44: ESP TN35000 pump strainer with ingested wire.

Photo 45: Ingested wire in bottom bowl assembly of test pump.

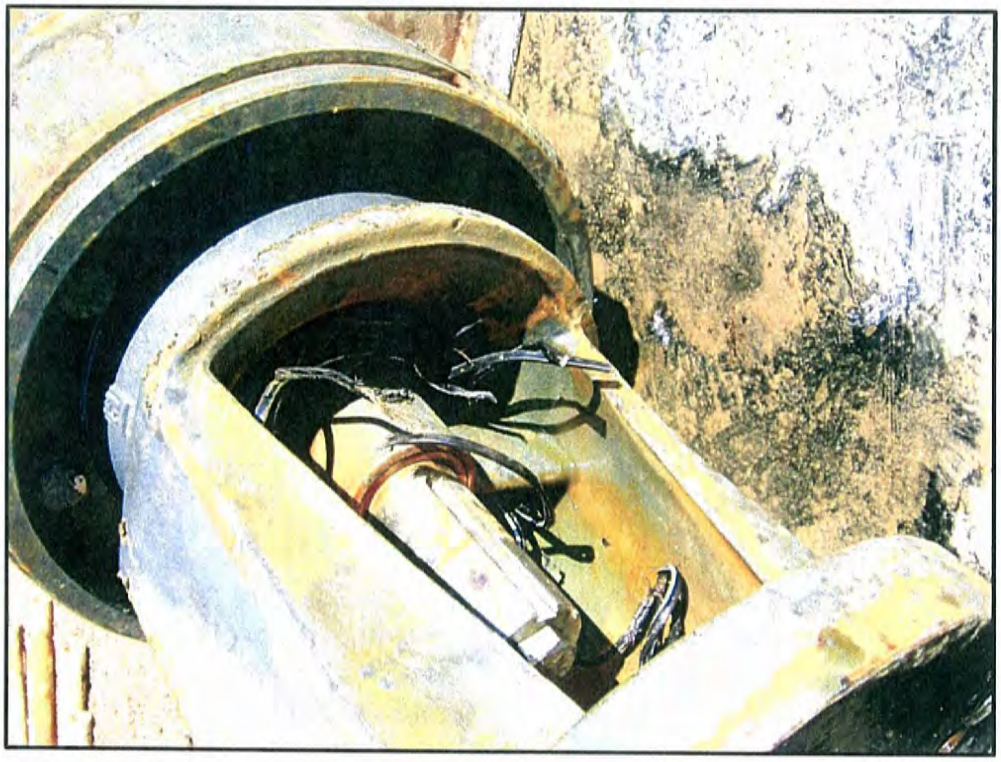

Figure 23: ESP TN 35000 pump performance summary.

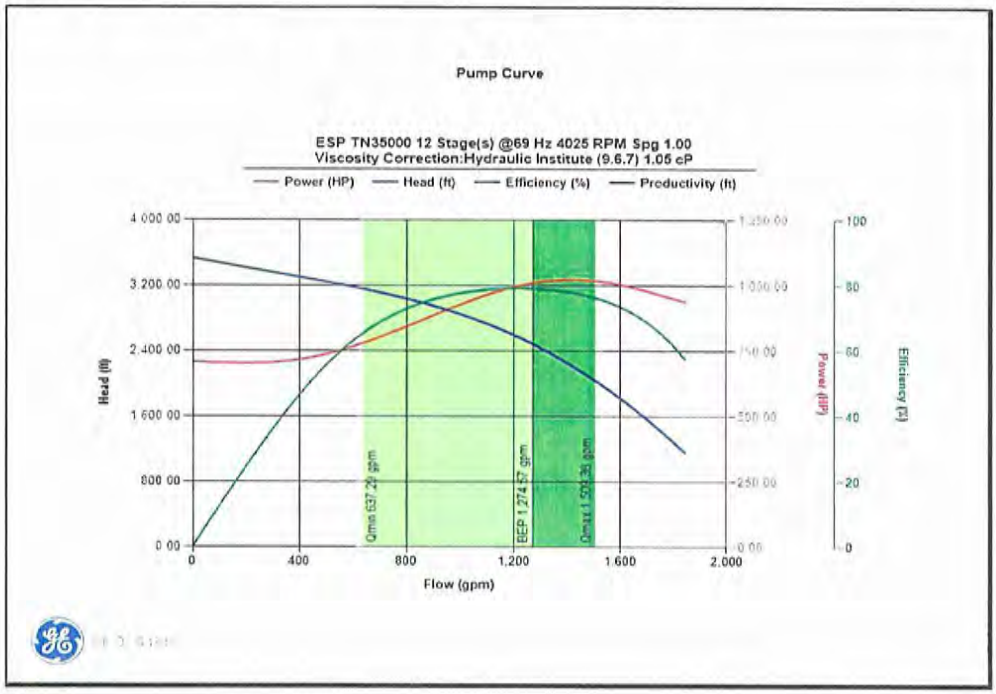

Figure 24: ESP TN35000 test pump VFD performance curves.

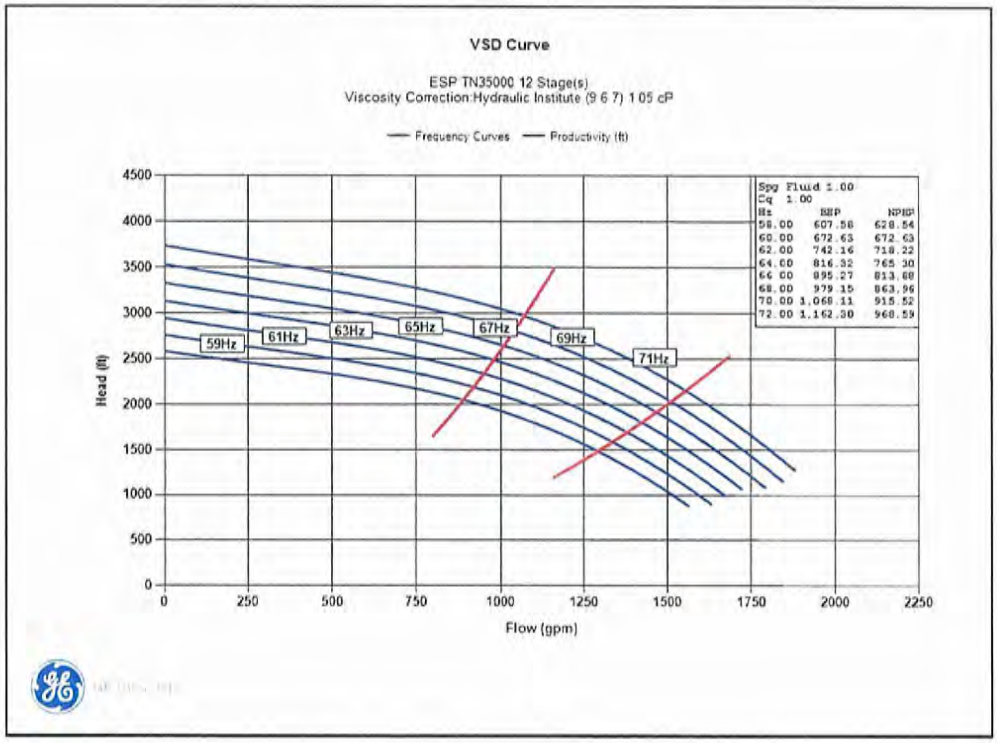

5.2.2 ESP TP1700 8-Stage Pump Curves

The pump inlet of the GE ESP TP1700 pump used in May 2013 was set at a depth of 1732.44 feet BGL in the 16-inch casing. The bottom of the pump motor was at a depth of 1804.17 feet BGL, 4.017 feet below the top of the 10-3/4 well casing which top is at 1800 feet.

Figures 25 and 26 show pump performance curves for the GE ESP TP1700 8-stage pump used for the 1600-gpm constant rate test of Test Well #1. Figure 25 indicates that the pump is capable of delivering 1600 gpm with 2200 feet of total dynamic head when operated at 60 Hz. Figure 25 also indicates the pump requires approximately 1070 horsepower to deliver the above performance. This exceeds the 1000-hp rating of the two 500-hp motors used in tandem to power this test pump; however, General Electric indicated that the two motors could be operated at up to 1100 hp, for more than three days of continuous pumping, provided the VFD were properly programmed for voltage and amperage limits. At 1100 hp and 60 Hz, Figure 25 indicates the pump can deliver 1700 gpm with approximately 2140 feet of total dynamic head.

Figure 25: ESP TP 1700 pump performance summary.

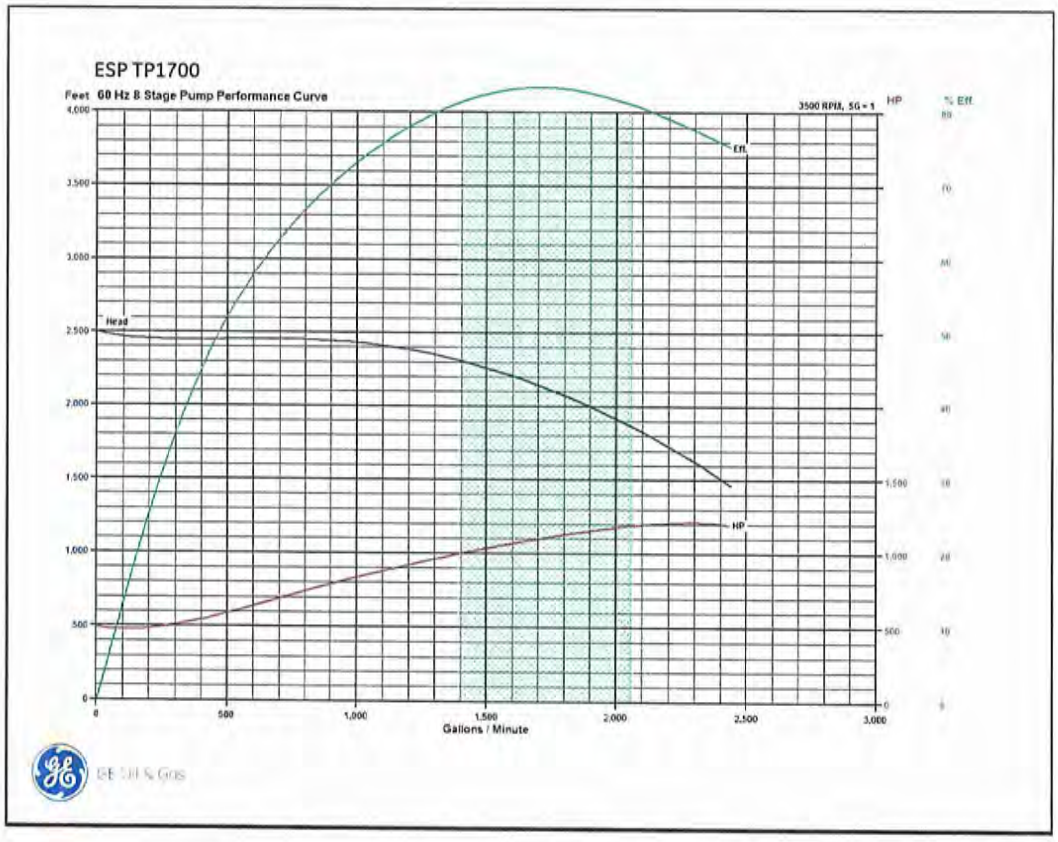

Figure 26: ESP TP1700 test pump VFD performance curves.

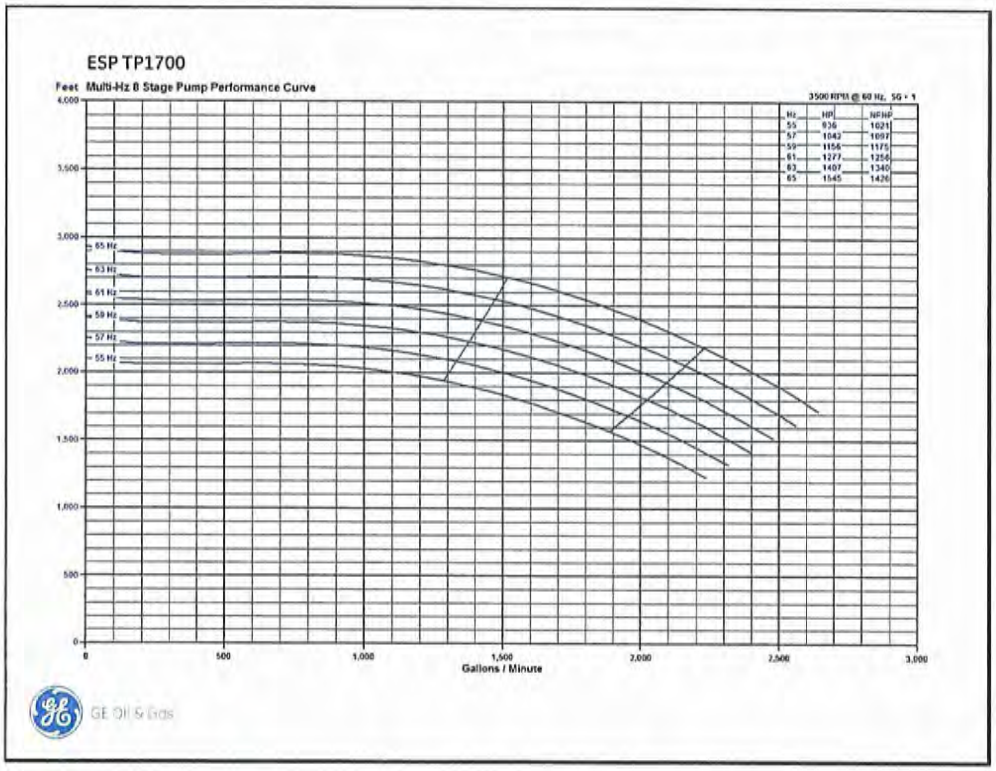

Figure 27: Pump performance curve compared to observed performance.

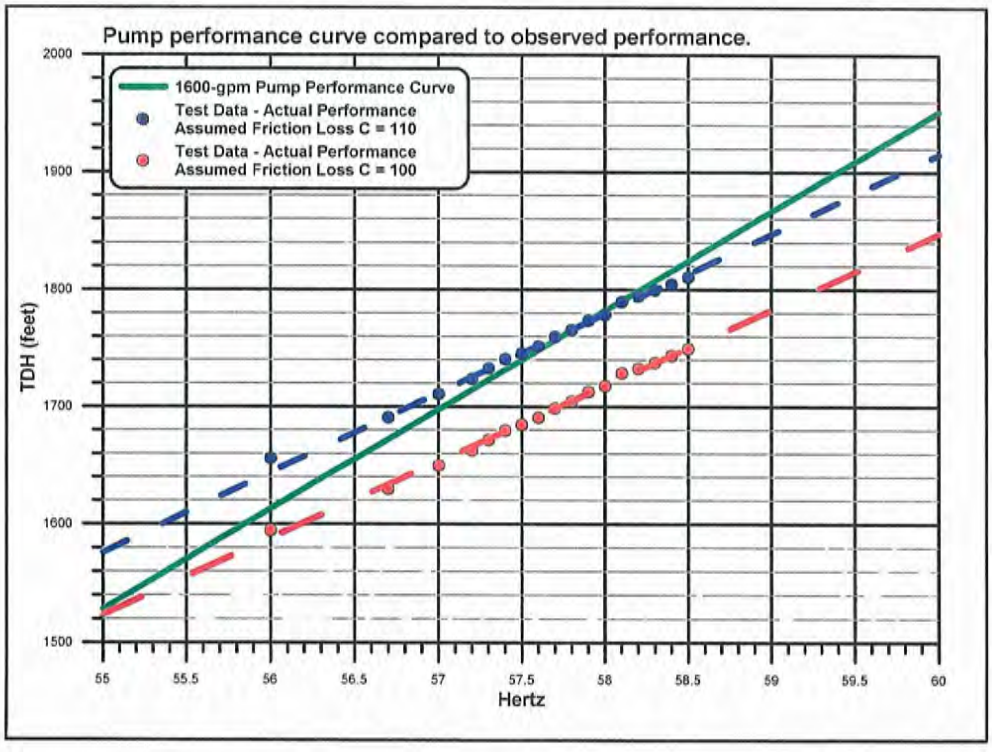

Photo 46: VFD secondary transformer data plate.

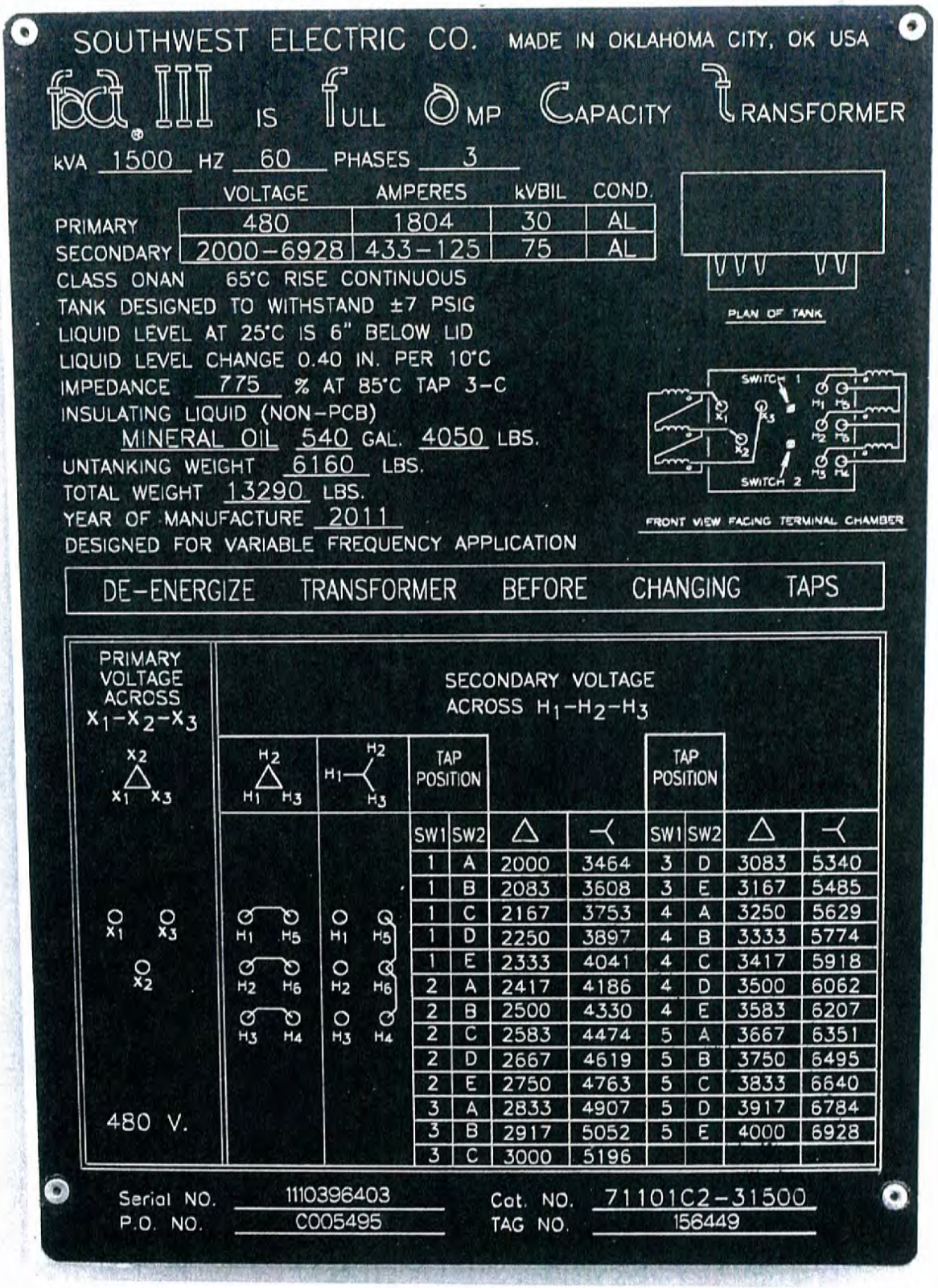

SOUTHWEST ELECTRIC CO. MADE IN OKLAHOMA CITY, OK USA

fda III IS FULL OMP CAPACITY TRANSFORMER

kVA 1500 HZ 60 PHASES 3

	VOLTAGE	AMPERES	kVBIL	COND.
PRIMARY	480	1804	30	AL
SECONDARY	2000-6928	433-125	75	AL

CLASS ONAN 65°C RISE CONTINUOUS
TANK DESIGNED TO WITHSTAND ±7 PSIG
LIQUID LEVEL AT 25°C IS 6" BELOW LID
LIQUID LEVEL CHANGE 0.40 IN. PER 10°C
IMPEDANCE 775 % AT 85°C TAP 3-C
INSULATING LIQUID (NON-PCB)
MINERAL OIL 540 GAL. 4050 LBS.
UNTANKING WEIGHT 6160 LBS.
TOTAL WEIGHT 13290 LBS.
YEAR OF MANUFACTURE 2011
DESIGNED FOR VARIABLE FREQUENCY APPLICATION

PLAN OF TANK

FRONT VIEW FACING TERMINAL CHAMBER

DE-ENERGIZE TRANSFORMER BEFORE CHANGING TAPS

PRIMARY VOLTAGE ACROSS $X_1-X_2-X_3$

480 V.

SECONDARY VOLTAGE ACROSS $H_1-H_2-H_3$

TAP POSITION				TAP POSITION			
SW1	SW2	Δ	Y	SW1	SW2	Δ	Y
1	A	2000	3464	3	D	3083	5340
1	B	2083	3608	3	E	3167	5485
1	C	2167	3753	4	A	3250	5629
1	D	2250	3897	4	B	3333	5774
1	E	2333	4041	4	C	3417	5918
2	A	2417	4186	4	D	3500	6062
2	B	2500	4330	4	E	3583	6207
2	C	2583	4474	5	A	3667	6351
2	D	2667	4619	5	B	3750	6495
2	E	2750	4763	5	C	3833	6640
3	A	2833	4907	5	D	3917	6784
3	B	2917	5052	5	E	4000	6928
3	C	3000	5196				

Serial NO. 1110396403
P.O. NO. C005495
Cat. NO. 71101C2-31500
TAG NO. 156449

The foregoing performance data assume the pump receives the necessary horsepower. In actual operation, this may not be the case because the VFD may be programmed to limit current draw by the motors in order to protect them from damage. This in turn may limit the horsepower delivered at any value of Hertz, thus not allowing the pump performance to achieve that shown on Figures 25 and 26. Figure 27 shows the pump performance (solid line), derived from Figures 25 and 26, from 55 to 60 Hz.

The observed pump performance on Figure 27 requires determination of total dynamic head for each data point. The pumping water level and pump column pressure are measured values; however, pump column friction loss must be calculated and the calculation required assumption of a "C" value or "roughness coefficient" for the inside of the pipe. A conservatively high amount of friction loss was used in the calculation by assuming a relatively rough steel pipe (consistent with the old and somewhat corroded pipe that was used) C value equal to 110. The observed data thus calculated plot in the same area as the theoretical pump curve, but have a different slope than the theoretical performance curve, and indicate the pump is likely underperforming compared to the theoretical curve, based on the slope of the curve for observed performance.

The observed performance curve slope will remain the same for different values of pump column pipe friction loss; however, changes in pump column pipe friction loss will shift the observed performance curve up and down the Y-axis of the plot on Figure 27. For example, a curve for observed performance is provided for an assumed C value of 100 for pump column friction loss. The latter curve is well below the published pump performance curve and demonstrates the sensitivity of the calculation to the assumed Hazen-Williams roughness coefficient ("C" value) for the pump column pipe.

5.2.3 Logging Equipment and Data Collection

Time-drawdown data were collected at one-minute intervals throughout the yield and drawdown tests. The water level data were collected and recorded by means of two 500-psi In-Situ Level TROLL 700 pressure transducers and loggers. One Level TROLL was installed in a PVC standpipe and the other was taped to the pump column; both installed to the top of the pump column collar immediately above the pump housing.

The static pressure over the pressure transducer on the pump column was 451.445 psi, on 3/7/2013, indicating the pressure transducer was 1041.84 feet below the static water level of 723.284 feet BTOC (top of standpipe) or at a depth of 1756 feet in the well, below the top of the standpipe. The Level TROLL 700 equipment was programed to collect depth to water, pressure on transducer and water temperature at a one-minute frequency for all tests.

The rate of flow was measured by a SITRANS F M MAGFLO MAG6000 flow meter, serial number 7ME692 677715N208 with a MAG51002 DN200 sensor, serial number 7ME658 066601D230. Full scale flow for water was 152.778 l/s (2421.5 gpm) and as shown on Figure 28, the meter was calibrated for 690 to 2072 gpm.

Figure 28: Calibration report for pumping test flow meter.

SIEMENS CALIBRATION REPORT

SITRANS F M MAGFLO

Customer			
Converter type	MAG6000	Serial No.	7ME692 677715N208
Sensor type	MAG5100W DN200	Serial No.	7ME658 066601D230
Cal. Factor	31.54572		
System Serial NO.	7ME658 021101U340		

Calibration Data

Full scale flow	152.7778	l/s	Calibration liquid	Water
			Calibration rig	RIG2

Calibration Settings

Frequency output	0-10000 Hz

Calibration Results

Test No.	Full scale flow	Water Temp	True Flow-Rate	Flowmeter Frequency output		
				Output	Flowrate	Error
	[%]	[°C]	l/s	[Hz]	l/s	[%]
1	90	-1.9	130.7245	8543.806	130.5304	-0.15
2	90	-1.9	130.6698	8559.218	130.7658	0.07
3	25	-1.9	43.5688	2854.120	43.6046	0.08
4	25	-1.9	43.5416	2855.082	43.6193	0.18
5						
6						
7						
8						
9						
10						

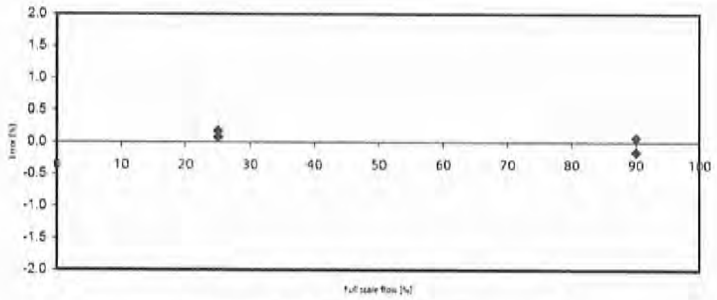

Calibrated by	hwl		
Date	2010-07-12	Time	07:42:00

The discharge rates during the stepped rate and constant rate tests were controlled by the flow meter which sent an analog signal to a PLC on the VFD controller to maintain a constant rate of flow for programmed rates. Pump column pressure was regulated by a gear-operated butterfly valve downstream from the flow meter.

5.3 Pre-Frac Pumping Tests

On 3/10/2013 at 9:10 A.M., the static water level in Test Well #1 was 724.773 feet below the top of a standpipe installed 23 inches above ground level which provides a static water level of 722.856 feet BGL.

5.3.1 Pre-Frac Stepped Rate Test

A stepped rate test began at a 500-gpm pumping rate at 9:10 A.M. followed by steps of 650, 800 and (nominally) 950 gpm. The steps were of 120-minute duration except for the 950-gpm step which exceeded the test pump capacity, resulting in an initial rate of 930 gpm which declined to 878 gpm in 23 minutes. Figure 29 shows the time-drawdown plots for each stepped rate.

Figure 29: Time-drawdown plots of pre-frac stepped rate test of Test Well #1.

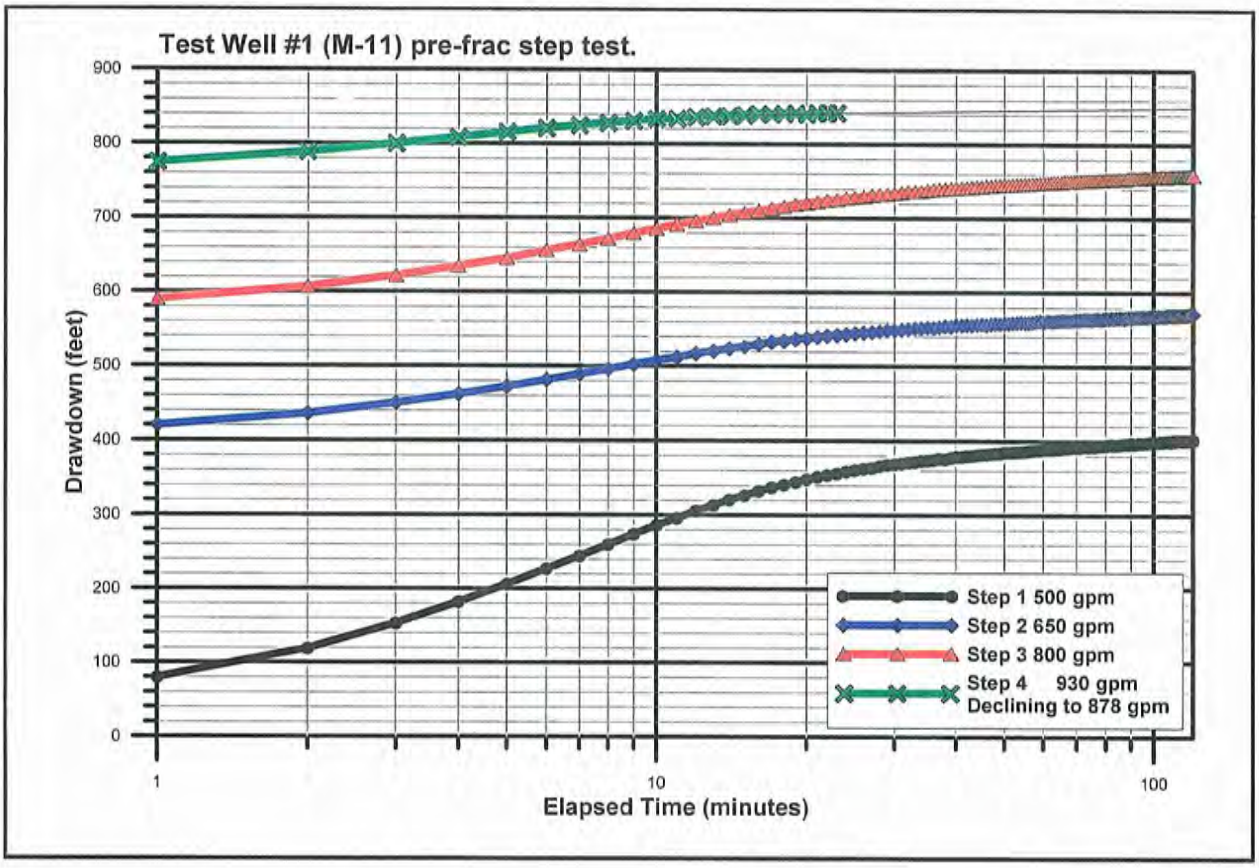

Data from the stepped rate test depicted on Figure 29 can be used for a conventional Hantush-Beirschenk analysis of well loss coefficients where total drawdown in a well, s_w, is determined for a given pumping rate, **Q**, for a specific pumping time by Equation 1, applying the well loss coefficients where B = linear well loss coefficient and C = nonlinear well loss coefficient.

Figure 30 shows a Hantush-Beirschenk plot of specific drawdown versus pumping rate on which the slope of a line through the data represents the coefficient "C" and the specific drawdown intercept of the line at zero pumping rate represents the coefficient "B". As shown on Figure 30, B = 0.5620637981 and C = 0.0004853475. The data point for the last step does not fall on the line because of the declining rate during that step.

Figure 30: Pre-frac Hantush-Beirschenk solution for Test Well #1.

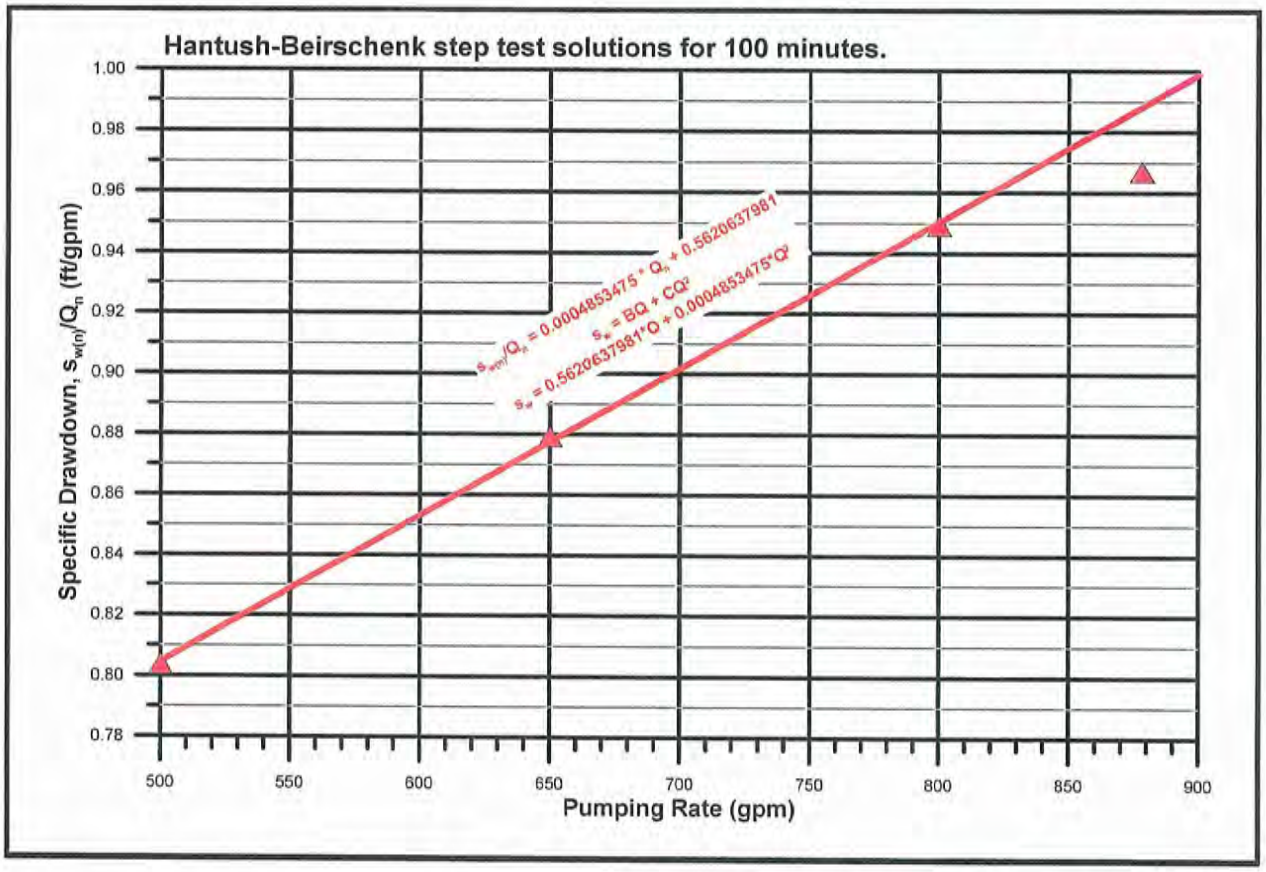

The well loss coefficients in Figure 30 are determined for 100 minutes of pumping duration. The well loss coefficients can be used to calculate the drawdown, s_w, for any reasonable range of pumping rates, using Equation 1 as shown on Figure 30. The well loss drawdown in the well is a constant for any constant rate of pumping. Therefore, the difference between the total drawdown calculated with Equation 1 and that predicted for aquifer drawdown based on aquifer hydraulic parameters (ideal drawdown) is the well loss for that pumping rate. The aquifer hydraulic parameters are determined from a constant rate test of the aquifer.

5.3.2 Pre-Frac Constant Rate Test

On 3/11/2013, a 900-gpm constant rate test of Test Well #1 was started. The test was performed for 12 hours, until the aquifer response was established. Figure 31 shows

the time-drawdown plot for the test, including residual drawdown during recovery plotted versus t/t' where t is time since pumping started and t' is time since pumping stopped. Fluctuations in drawdown are reflected on the time-drawdown curve between 100 and 150 minutes and are attributed to transient development of the porous to cavernous formation; however, the Rossum sand tester did not register any sediment during this period of time, indicating the sediment was too large to enter the ¼-inch pipe to the sand tester. This is typical of hard carbonate rock where the sediment was likely limestone cuttings that are too large to enter the sand sampler.

Figure 31: Pre-frac 900-gpm constant rate test of Test Well #1.

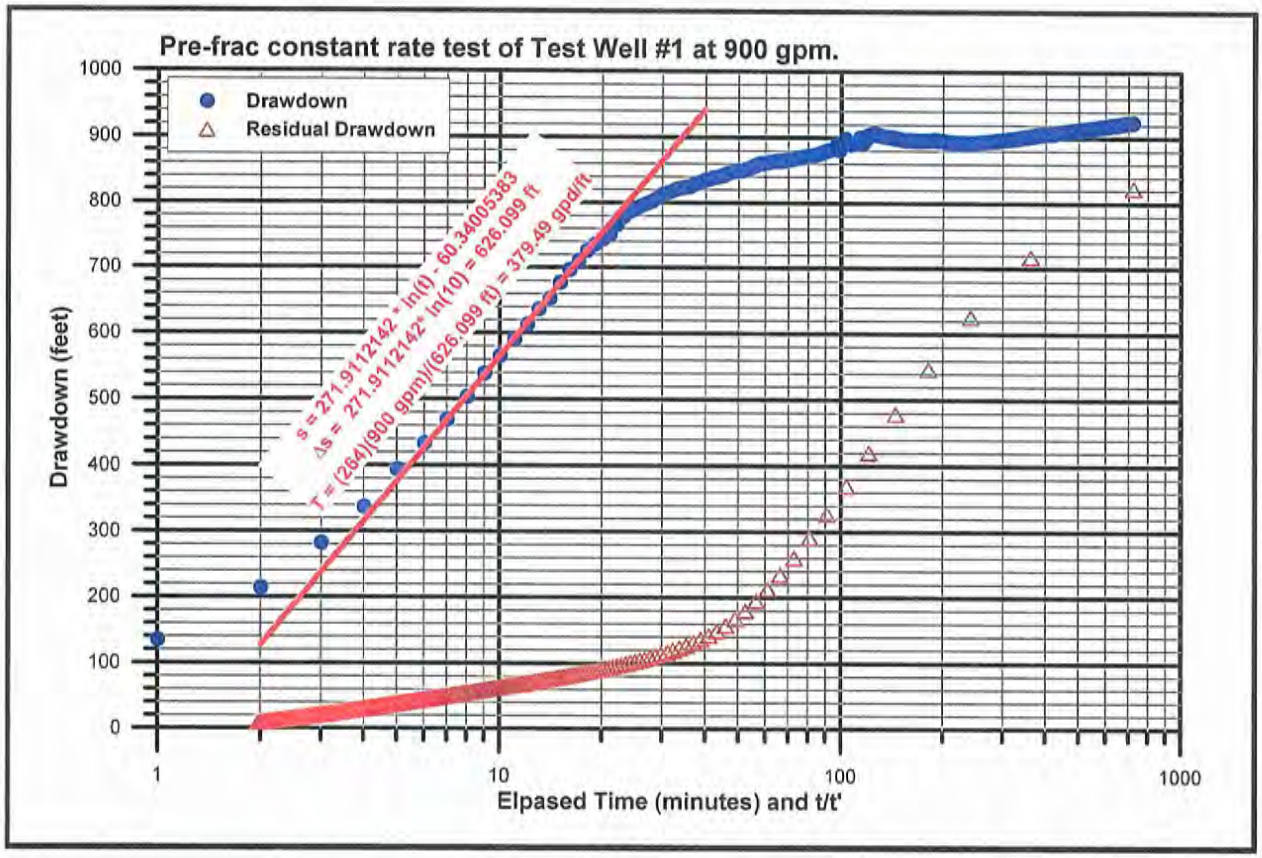

Figure 31 shows a Cooper-Jacob solution for the aquifer transmissivity, calculated from the drawdown over one log cycle of pumping time. The rate of drawdown over one log cycle of pumping time is determined from the data from 7 to 17 minutes of pumping time and provides a value of aquifer transmissivity of 379 gpd/ft (50.7 ft^2/day). After approximately 20 minutes of pumping time, a sudden decrease in the slope of the time-drawdown data indicates the onset of a recharge effect. The recharge is provided by release of groundwater from storage in a nearby high-conductivity fracture.

Figure 32 shows a semilogarithmic plot of the Theis type curve. Figure 32 shows that by the middle of the second log cycle of the type curve, the semilogarithmic line can be approximated with a semilogarithmic straight line, although it does in fact exhibit a small

amount of curvature. The approximation of the type curve by a semilogarithmic straight line becomes better as $1/\mu$ increases (μ decreases). It is for this reason that the Cooper-Jacob straight-line solution was historically applied only when $1/\mu \leq 0.01$ or $\mu \geq 100$; however, this is a very rigid criteria and it is evident on Figure 32 that the type curve can be fairly well represented with a straight line for values of μ as small as 5.0 ($1/\mu = 0.2$) with no more than 5 percent error. Comparison to the ideal radial flow time-drawdown response on Figure 32 to the 7 to 17-minute data on Figure 31 indicates that unless the cone of depression around Test Well #1 impinged on either a decrease in aquifer transmissivity or a source of recharge, it would not depart from the

Figure 32: Semilogarithic plot of Theis type curve.

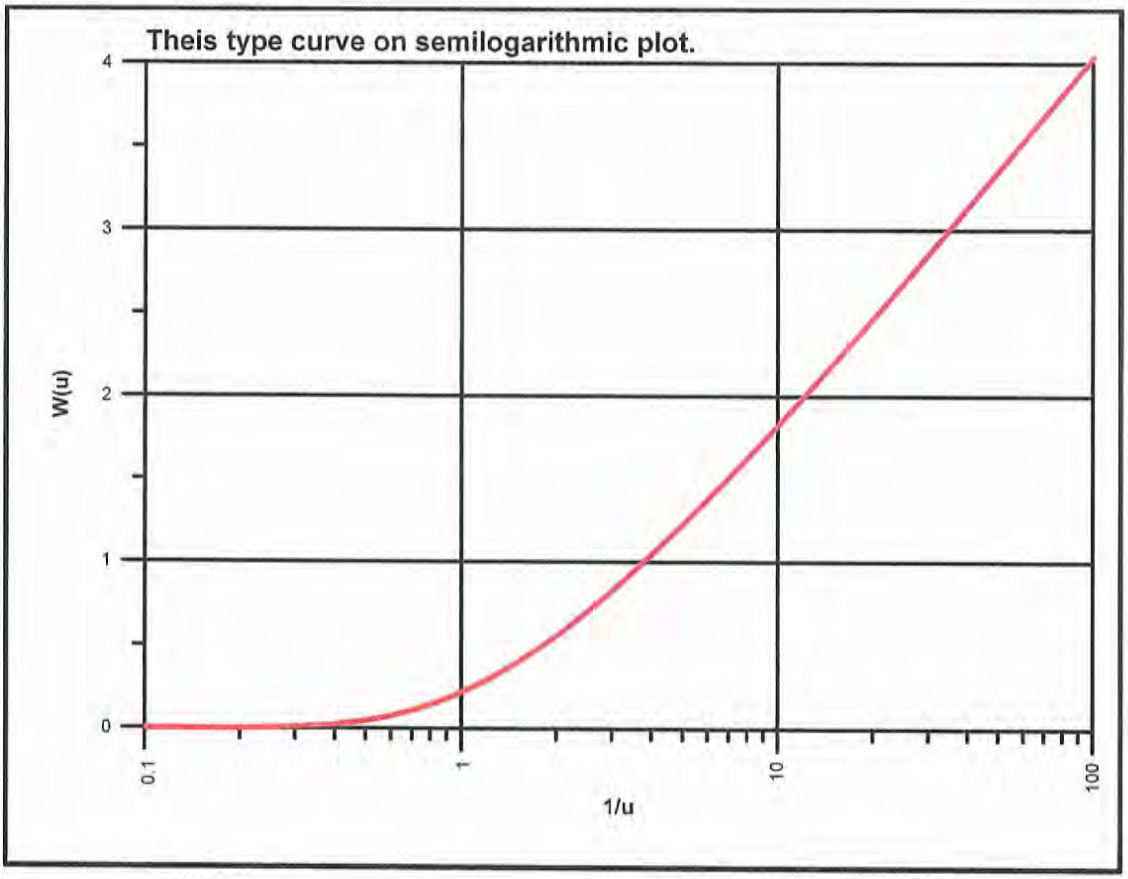

semilogarithmic straight line response. This indicates the solution provided on Figure 31 is valid and compares to the first 1.5 to 2.0 log cycles of time on the type curve on Figure 32. The potential error due to representing a curved line with a straight line is no more than 5 percent and the fit of the straight line to the 10 data points provides an R-squared value of 0.999.

If the Cooper-Jacob solution provided on Figure 31 is correct, the transmissivity value, 379.45 gpd/ft, can be applied in the Theis non-equilibrium equation to predict drawdown at any pumping rate and duration. The drawdown predicted by the Theis non-

equilibrium equation will not include well loss drawdown. Since residual drawdown during recovery does not include well loss, the Theis model prediction should closely match the residual drawdown data. Figure 33 shows the Theis model output for a 900-gpm pumping rate compared to the field data from the 900-gpm test. The Theis data reasonably match the residual drawdown, thus verifying that 370.45 gpd/ft is a reasonable value for the aquifer transmissivity.

Figure 33: Theis model output for 900 gpm compared to field data.

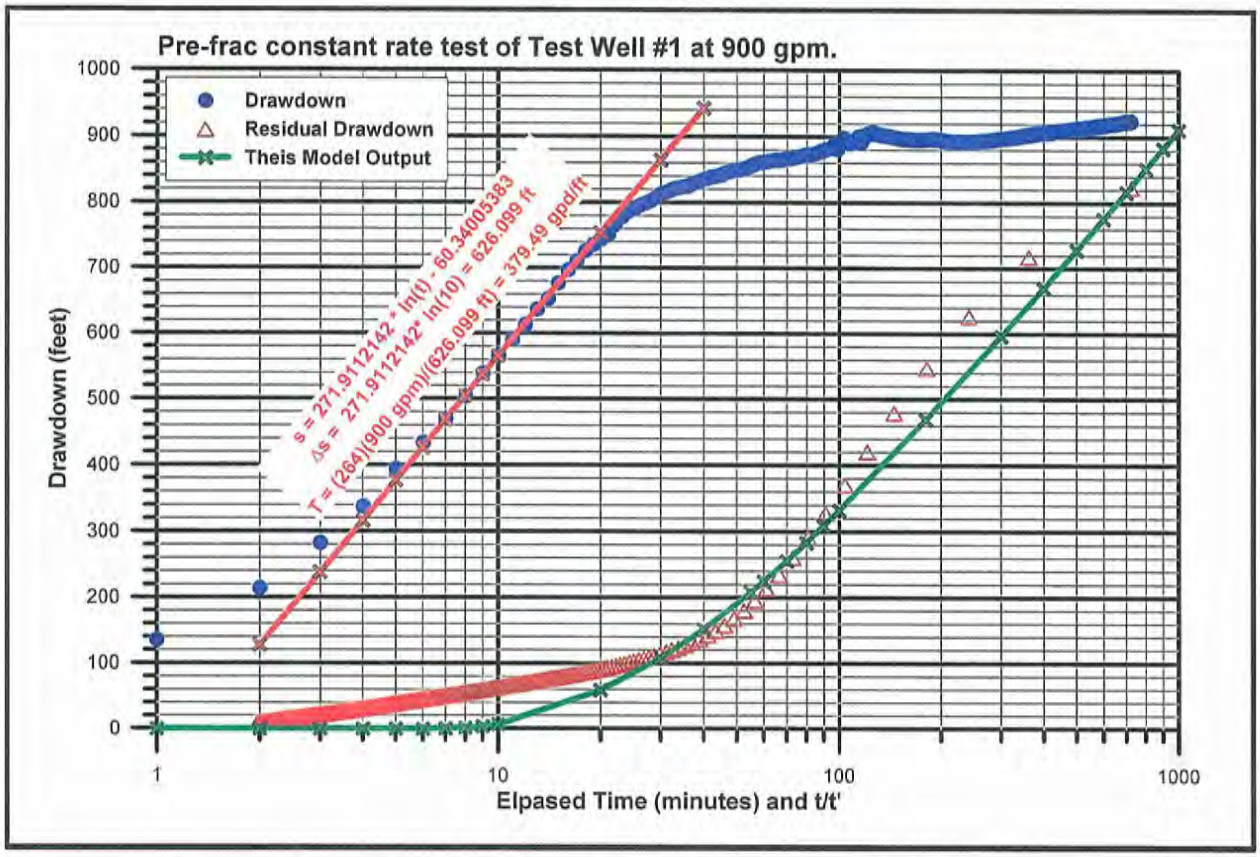

The apparent difference between the Theis model output and the semilogarithmic regression line through the early drawdown data is partly due to the previously discussed problem of representing a slightly curved log-log line on a semi-log plot with a semi-log straight line. However, the residual drawdown has a slightly steeper slope than the drawdown, if the first value of residual drawdown after the pumping stops is ignored. The fact that the Theis model output plots right on the first data point for recovery suggests the difference in slope between drawdown and residual drawdown is due to casing storage effects, without which there would be little difference between the model output and the observed residual drawdown.

5.3.3 Aquifer Parameters

In summary, the pre-frac constant rate early test response at Test Well #1 at 900 gpm indicates an aquifer transmissivity of 379.45 gpd/ft (50.72 ft^2/day). The aquifer storativity is not determined because it is not possible to determine aquifer storativity without an observation well. Test Well #2A was used as an observation well; however, valid aquifer parameters could not be determined at Test Well #2A.

The pre-frac response of Test Well #2A to the 900-gpm constant rate test of Test Well #1 is shown on Figure 34 as a log-log plot so that a log-log Theis type curve can be fit to the data. For the first 150 minutes of the test the response is too small to measure reliably; then the aquifer drawdown becomes large enough to resolve with the 500-psi pressure transducer used for the test. A Theis type curve is fit to the data and a match point and solution for aquifer transmissivity and storativity are shown.

Figure 34: Pre-frac response of Test Well #2A to 900-gpm test of Test Well #1.

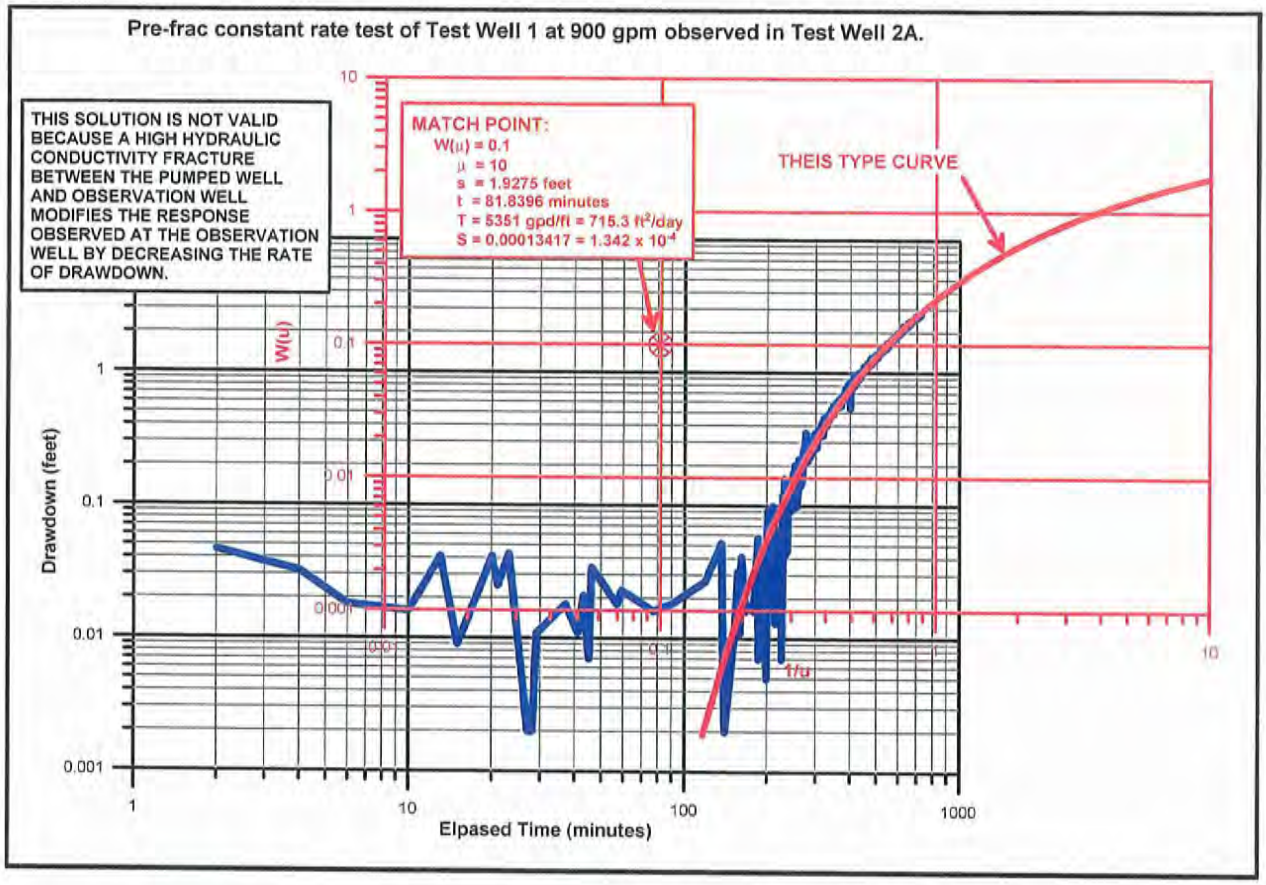

The Theis solution on Figure 34 provides a transmissivity value that is an order of magnitude larger than that at the pumped well. This is because the rate of drawdown observed in Test Well #2A was reduced by the release of water from storage in a high hydraulic conductivity fracture that is located between Test Well #2A and the pumped well, Test Well #1. The resultant decrease in the slope of the time-drawdown curve at

the observation well results in derivation of an erroneously large value of aquifer transmissivity from the test data at the observation well. Another way of looking at this is that the effective pumping rate affecting Test Well #2A is considerably less than the 900 gpm rate at pumped Test Well #1 due to recharge from the fracture providing part of the water pumped from Test Well #1.

5.4 Post-Frac Pumping Tests

On 3/26/2013, Test Well #1 was subjected to stimulation with high-pressure, high-volume hydrochloric acid. After a small pump was used to pump post-frac water to frac tanks and water was hauled off site until the pH of the discharge water was verified to be 6.5 standard pH units or greater, the test pump was reinstalled, and a stepped rate test of the well was conducted on 4/13/2013. Stepped rate testing was followed by a 1600-gpm constant rate test of 81 hours duration which started on 5/10/2013.

5.4.1 Post-Frac Stepped Rate Test

Figure 35 shows the response of the well to pumping at six progressively increased pumping rates, each for a minimum duration of 120 minutes except for the 1605 gpm rate where the VFD ramped the rate back to 1475 gpm after 78 minutes of pumping at 1605 gpm, when the pump motor current draw exceeded a pre-set limit of 150 amps. It is also evident that after about 10 minutes of pumping, the 1605-gpm rate began to decrease in response to reaching the limits of the VFD and generator programming.

Standard Hantush-Beirschenk solutions for well loss coefficients were applied to the stepped rate test data shown on Figures 29 and 35 for pre-frac and post-frac stepped rate tests. Figure 36 shows the solutions for pre-frac and post-frac well loss coefficients.

Figure 36 exhibits a considerable decrease in specific drawdown ($s_{w(n)}/Q_n$) between pre-frac and post-frac conditions; indicating the success of acid-treatment of the well in reducing well loss drawdown. The equation on Figure 36 for post-frac conditions can be used to predict the total drawdown, s_w, of the well for any given pumping rate, at a constant rate of pumping for 100 minutes. Since well loss is constant, well loss can be determined at any pumping rate by subtracting the predicted aquifer drawdown for 100 minutes from the predicted total drawdown for 100 minutes.

The well loss coefficients for post-frac conditions in Test Well #1 are as follows:

$$B = 0.1841721675$$
$$C = 0.0001366748166$$

After the 4/13/2013 stepped rate test, plans were made to repeat the test with the VFD set to run the submersible pumps at 110 percent of rated horsepower or 1100 hp with the VFD set to a limit of 164 amps. The repeat step test was initiated at 9:00 A.M. on 4/16/2013. The pump discharge ramped up to approximately 1000 gpm by 9:03 A.M. and then in the next minute decreased to 20 to 50 gpm fluctuations. The decrease in

Figure 35: Post-frac stepped rate test of Test Well #1.

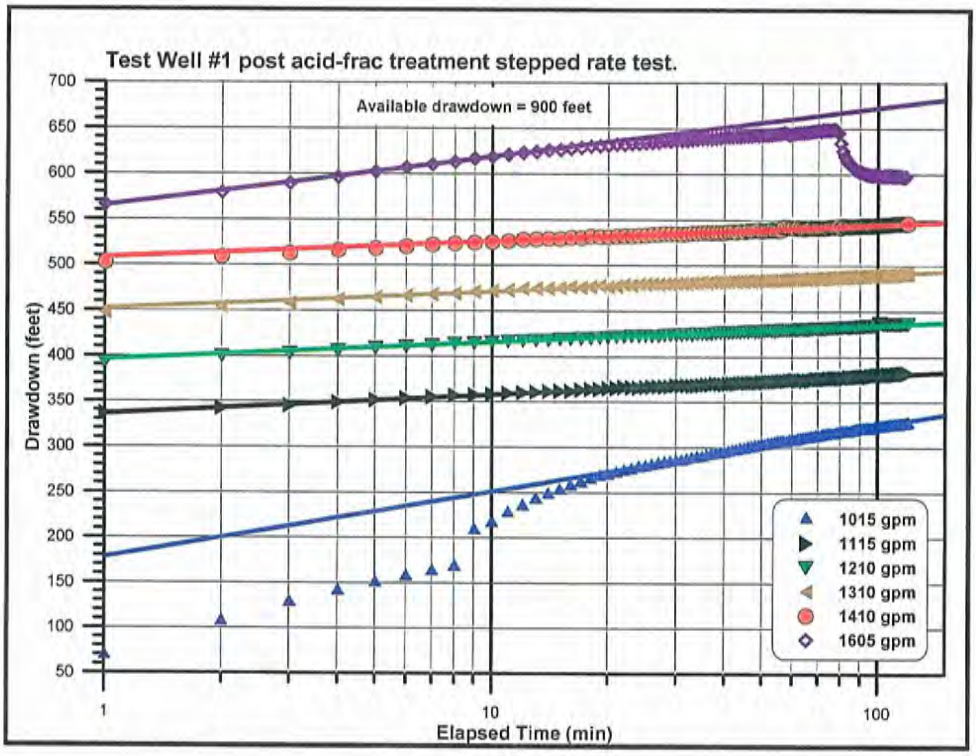

Figure 36: Well loss coefficient solutions for pre- and post-frac stepped rate tests of Test Well #1.

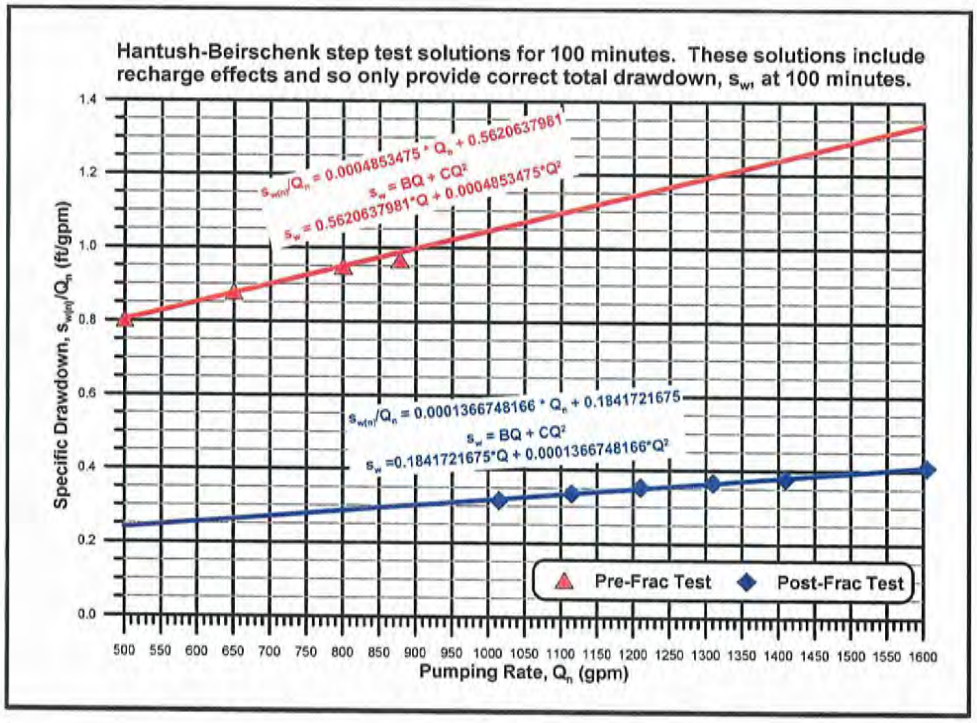

pumping rate displayed by the flow meter was verified by visual inspection of the discharge. The pump was stopped and repeated efforts to start the pump again resulted in a discharge rate of about 20 gpm. It was subsequently found that the pump had ingested a large length of water level indicator wire that had been lost in the well during the previous stepped rate test (Photos 44 and 45).

Photo 47 shows limestone cuttings, as well as copper wire strands and fragments of wire insulation, found on the check valve in the pump column after removal of the pump,

Photo 47: Limestone cuttings developed from Test Well #1 after acid-frac treatment.

thus verifying earlier speculation that the well was continuing to develop, as shown on Figure 31. The development consisted of the removal of limestone cuttings remaining after the air rotary drilling of the open-completion borehole. This indicates the need to provide additional development of the well by air lift pumping, after total depth is reached and again after acid-frac stimulation of the well.

5.4.2 Post-Frac Constant Rate Test

The 12-stage pump damaged by the ingested wire was replaced with the original 8-stage GE ESP TP1700 pump, which had been repaired. In view of the amount of drill cuttings observed on the pump column check valve during removal of the failed pump, and the evidence of wear of the pump bowl housing from previous tests in the City of Gillette test wells, it was decided to limit testing to a 1600-gpm constant rate test of Test Well #1, to limit the risk of pump failure due to wear by sediment, and to increase the likelihood of successful completion of a constant rate test before the pump experienced excessive wear.

Figure 37 shows a semilogarithmic plot of the time-drawdown and residual drawdown data from the 81-hour constant rate test, including a Cooper-Jacob straight-line solution for aquifer transmissivity. The post-acid frac stimulation value of transmissivity is 1310 gpd/ft.

Figure 37: Cooper-Jacob solution for 1600-gpm post-frac test of Test Well #1.

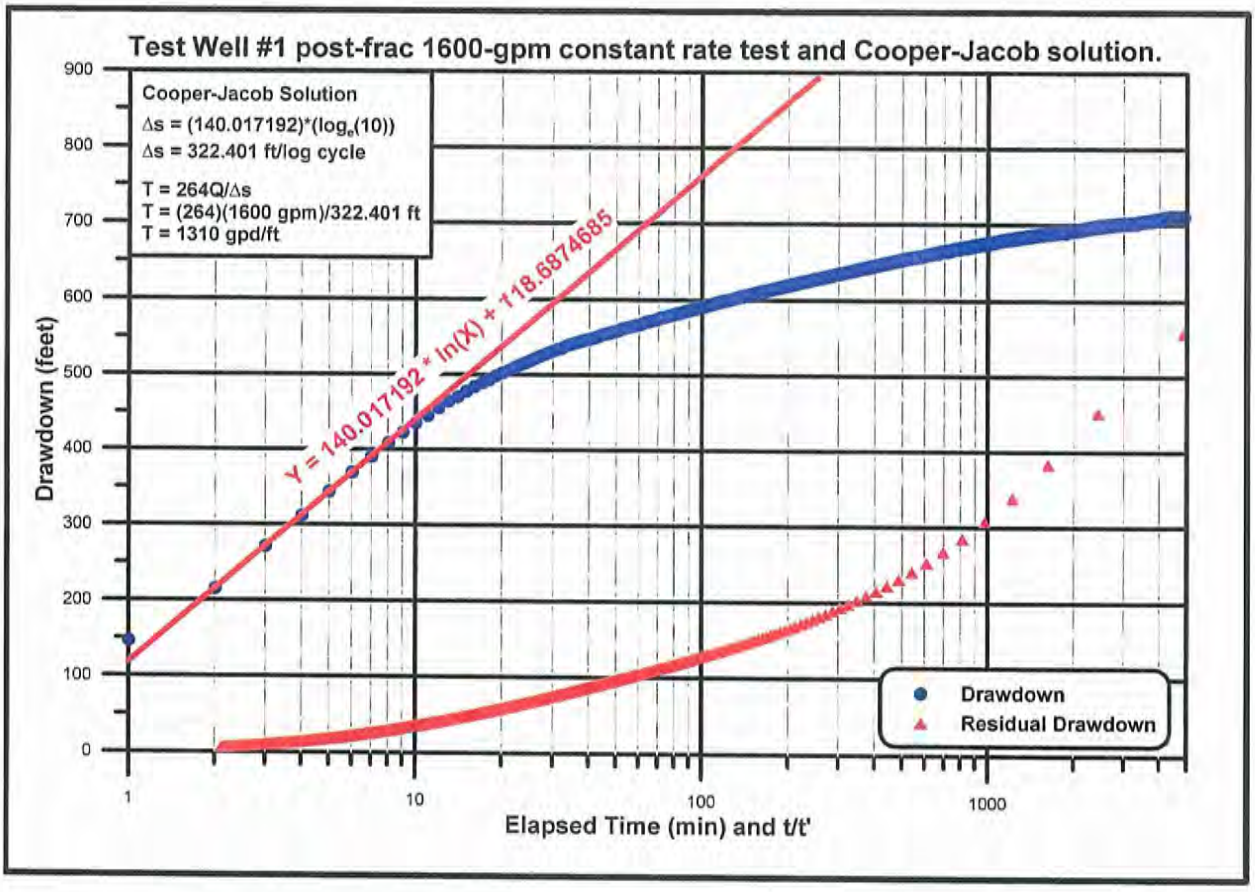

Similarly to the pre-frac 900-gpm test, the Theis non-equilibrium equation should replicate the residual drawdown for the 1600-gpm test, if the 1310-gpd/ft value of transmissivity is used in the Theis model. Reasonable reproduction of the residual

drawdown by the Theis model validates the solution for transmissivity. Figure 38 shows the Theis model output, based on a transmissivity value of 1310 gpd/ft, compared to the drawdown and residual drawdown. It is readily apparent that the Theis model output is reasonably parallel to the Cooper-Jacob regression line through the drawdown data; however, it does not compare favorably to the residual drawdown data. Residual drawdown is less than the Theis model output throughout the plot, thus indicating that essentially all of the drawdown data during the post-frac, 1600-gpm test were affected by recharge. Accordingly, the 1310 gpd/ft value of transmissivity is not valid for the aquifer.

Figure 38: Theis model output compared to 1600-gpm test response.

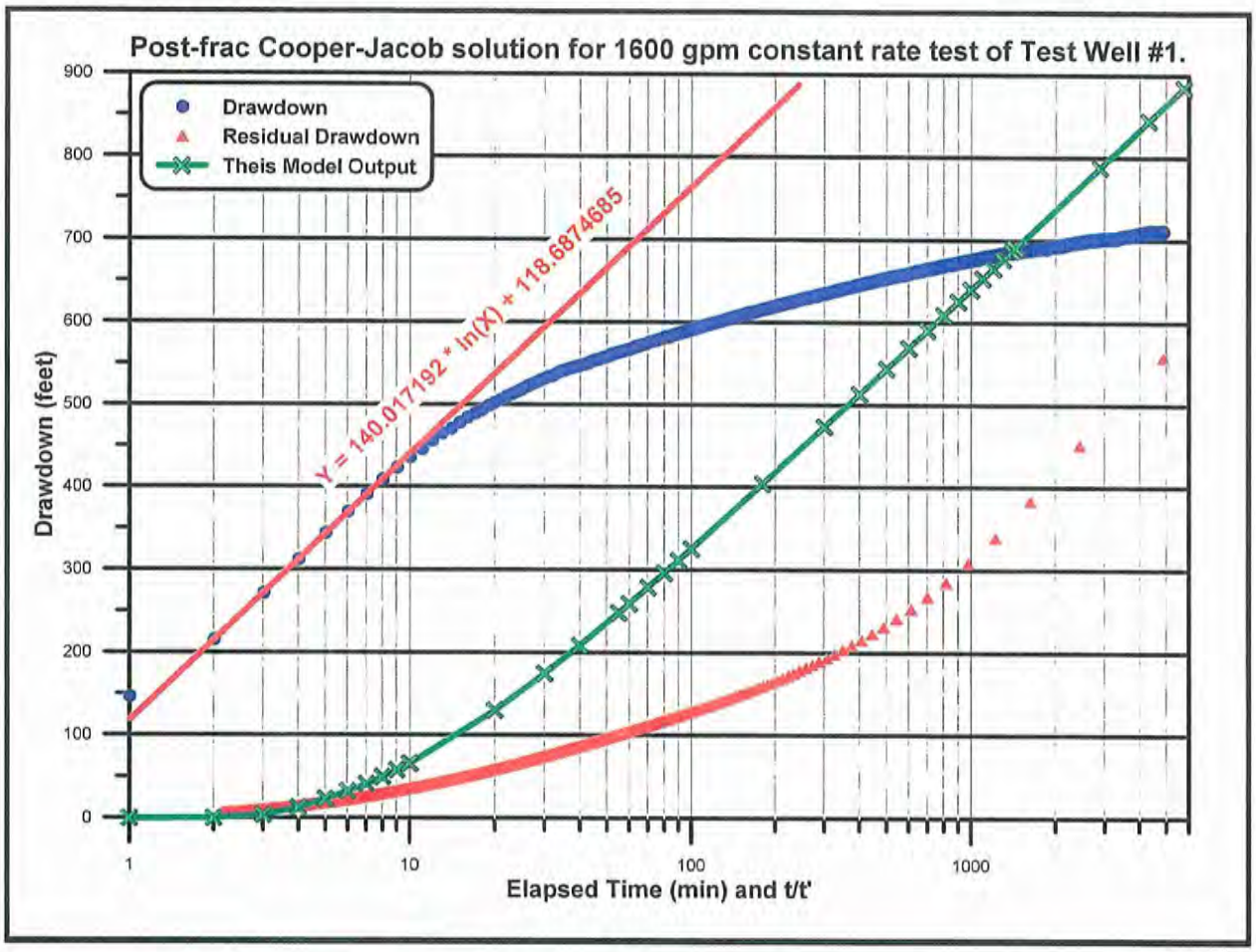

5.4.3 Stabilized Drawdown

The 1600-gpm constant rate test shows the influence of a recharge boundary beginning at 10 minutes of elapsed pumping time. The recharge boundary persists throughout the remainder of the pumping test, and is interpreted to indicate the presence of a high-conductivity, solution enlarged fracture within the area of aquifer depressurized by the 1600-gpm pumping rate. As shown on Figure 39, the rate of drawdown stabilizes

during approximately the last 500 minutes of the 1600-gpm pumping test. The stabilization of the drawdown, as well as other fluctuations in the drawdown, are not related to barometric fluctuations during the test and indicate the recharge received from the solution enlarged fracture equaled the pumping rate. In other words, release of groundwater storage from the hypothesized high-conductivity fracture provided all of the pumped water after drawdown at the pumped well stabilized.

Figure 39: Stabilized drawdown at end of 1600-gpm constant rate test of Test Well #1.

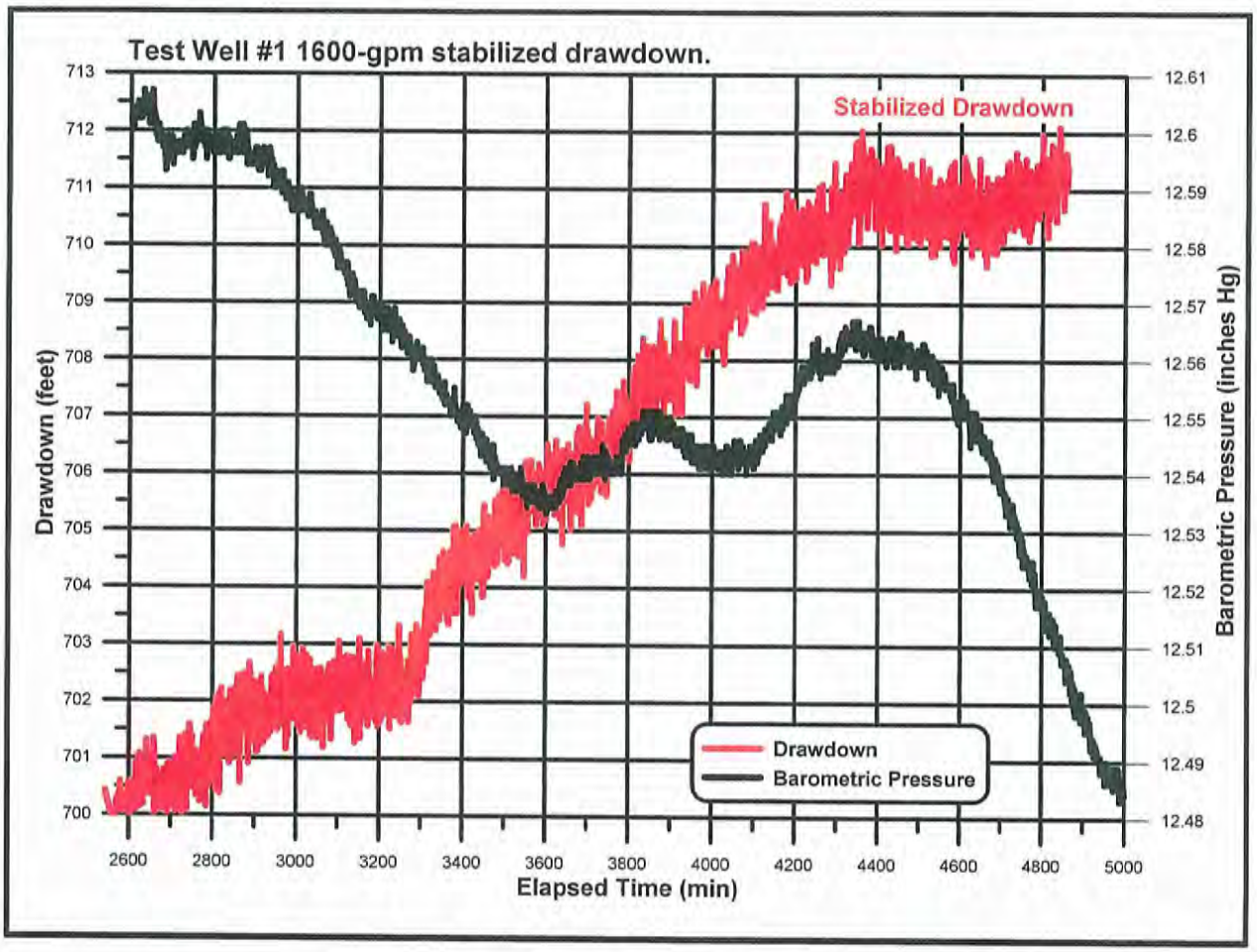

A Theis solution is not shown for the 1600-gpm test at the pumped well. This is because it is established in the Cooper-Jacob straight-line solution that essentially all of the 1600-gpm test data are influenced by a recharge boundary.

5.4.4 Post-Frac Observation Well Response

Figure 40 shows the response observed in Test Well #2A when Test Well #1 was pumped at 1600 gpm for 81 hours. The data are presented in a diagnostic log-log plot where a log-log straight line is diagnostic of a rate of drawdown controlled by the release of stored groundwater from a linear feature. Linear features may include strip

aquifers, such as sand and gravel streambed alluvium bounded by relatively impervious bedrock, open underground mine workings below the water table, shear zones in hard crystalline rock, permeable igneous dikes bounded by less permeable host rock and

Figure 40: Response of Test Well #2A to 1600-gpm pumping rate at Test Well #1.

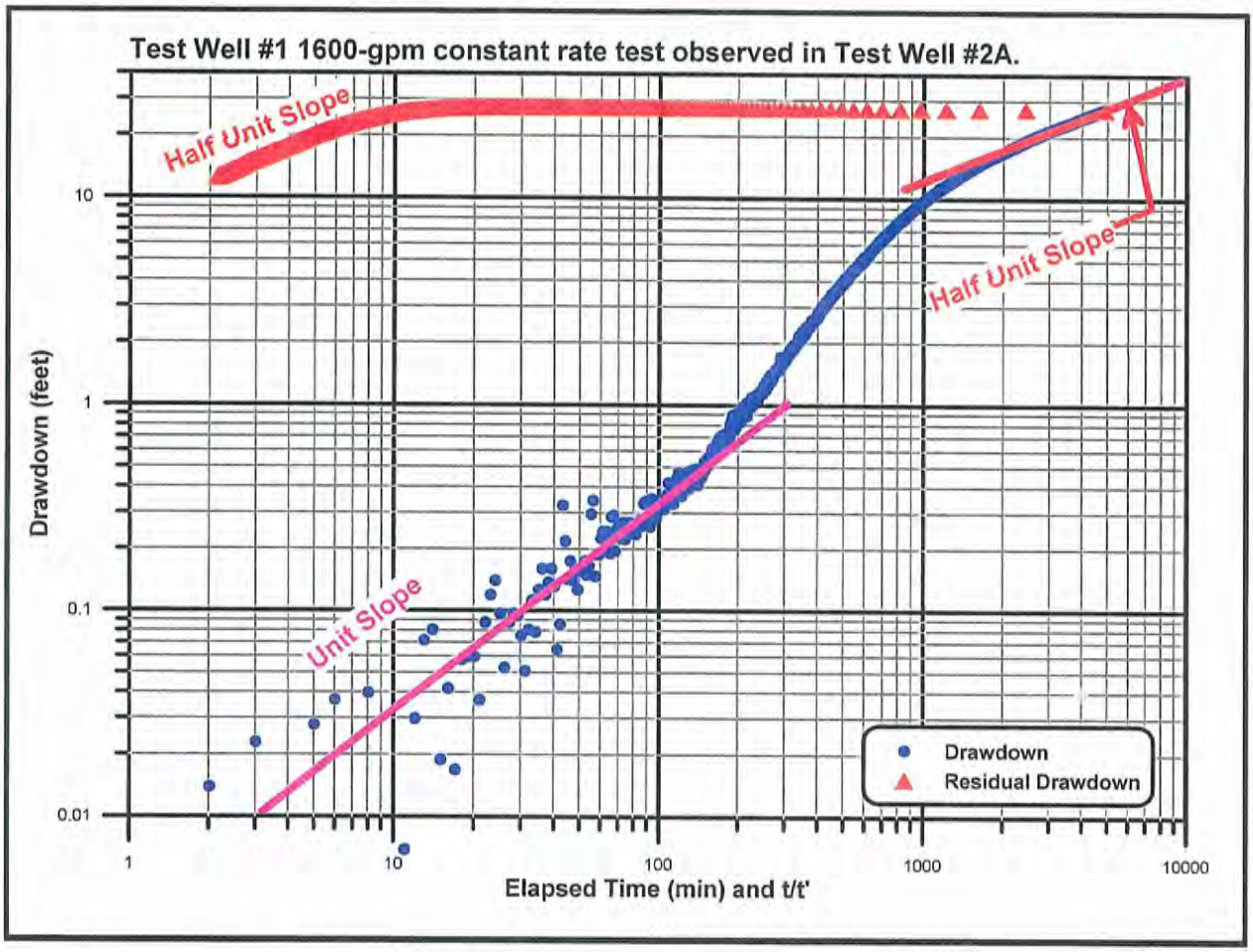

solution enlarged fractures in soluble carbonate rock. Wells penetrating any of the foregoing features may exhibit one or more phases of linear flow which produces log-log time-drawdown straight lines of different slopes. All linear flow features have in common the properties of storage of groundwater within their boundaries and the control of the rate of drawdown in pumped wells by the manner in which release of that storage occurs. Likewise, they all exhibit non-uniform drawdown, i.e., a groundwater gradient develops along the length of the linear feature and is graded to the pumped well. These linear features are distinctly different than high- and low-conductivity, single vertical and horizontal fractures described in the literature that have uniform drawdown and no storage properties. The published solutions for drawdown response in the latter features do not apply to the features near Test Well #1 which offer groundwater storativity and longitudinal hydraulic gradients during pumping.

The initial response in Test Well #2A is approximately half a foot of drawdown over a period of 146 minutes, during which time the rate of drawdown is a log-log unit slope, i.e., one log cycle of drawdown per one log cycle of time. This early portion of the response records the initial impingement of the radial flow cone of depression around the pumped well upon the high-conductivity linear fracture. Unit slope response begins in the earliest data, indicating the fracture responds almost as soon as the pump starts and modifies the response at the observation well, which is on the opposite side of the fracture from the pumped well, at the very beginning of the test. The unit slope response indicates a period of time during which drawdown impinging on the fracture and drawdown within the fracture are so small as to cause essentially uniform drawdown in the fracture, as groundwater storage in the fracture flows into the radial flow cone of depression, with the radial flow cone of depression distributed along a length of the fracture and essentially no hydraulic gradient developed in the fracture.

The unit slope response is followed by a period of transition from a unit slope response to a half unit slope response (two log cycles of time for one log cycle of drawdown). The transition indicates the gradual development of a hydraulic gradient along the fracture, presumably to the center of the radial flow cone of depression where it was tangent to the fracture.

The half unit response indicates that the rate of drawdown observed in Test Well #2A is controlled by the release of groundwater stored in the fracture. The groundwater released from the fracture is flowing into the radial flow cone of depression and to the pumped well, just as it is during the unit slope and transitional portions of the response.

Figure 40 shows that after pumping ceased, the groundwater level in Test Well #2A continued to decline for nearly 5.5 hours, before the groundwater level in the well began to rise. This continued decline in the groundwater level after the pump stopped is evident in the residual drawdown response on Figure 40 wherein the drawdown increases to a t/t' value of about 13.6 or 6.4 hours after the pump was stopped. The period of continued decline in the groundwater level at Test Well #2A after pumping at Test Well #1 records the period of time required to restore the water level in the cone of depression between the pumped well Test Well #1 to a level equal to that in the fracture so that recovery of the water level in the fracture can begin. After the water level in the fracture begins to recover, it recovers at a half unit slope rate (Figure 40 where t/t' is less than 10), indicating that the restoration of the groundwater storage in the fracture is controlling the rate of recovery in the porous carbonate aquifer at Test Well #2A.

Figure 41 is a hydrograph of the depth to water in Test Well #2A during the pumping and recovery of Test Well #1. The pre-test groundwater level declines about 3.3 feet overnight due to pumping conducted the previous day at Test Well #1 to set up the pump and VFD controls. The pumping period shown is 81 hours and 72 hours of recovery are shown as residual drawdown, including the 6.5 hours of declining groundwater levels after the pump was stopped. Some 12.54 feet of residual drawdown remain after 72.1 hours of recovery. Moreover, the trend of recovery of the residual drawdown does not indicate that the local water level in Test Well #2A will recovery to

the initial pre-test level in any reasonable period of time, and certainly not in a period of time that is equal to the preceding pumping duration. Crude projection of the trend suggests approximately 10 feet of residual drawdown will remain at Test Well 2A long after pumping of Test Well #1 at 1600 gpm for 81 hours has ceased.

Figure 41: Hydrograph of Test Well #1 response to 1600-gpm pumping in Test Well #2A.

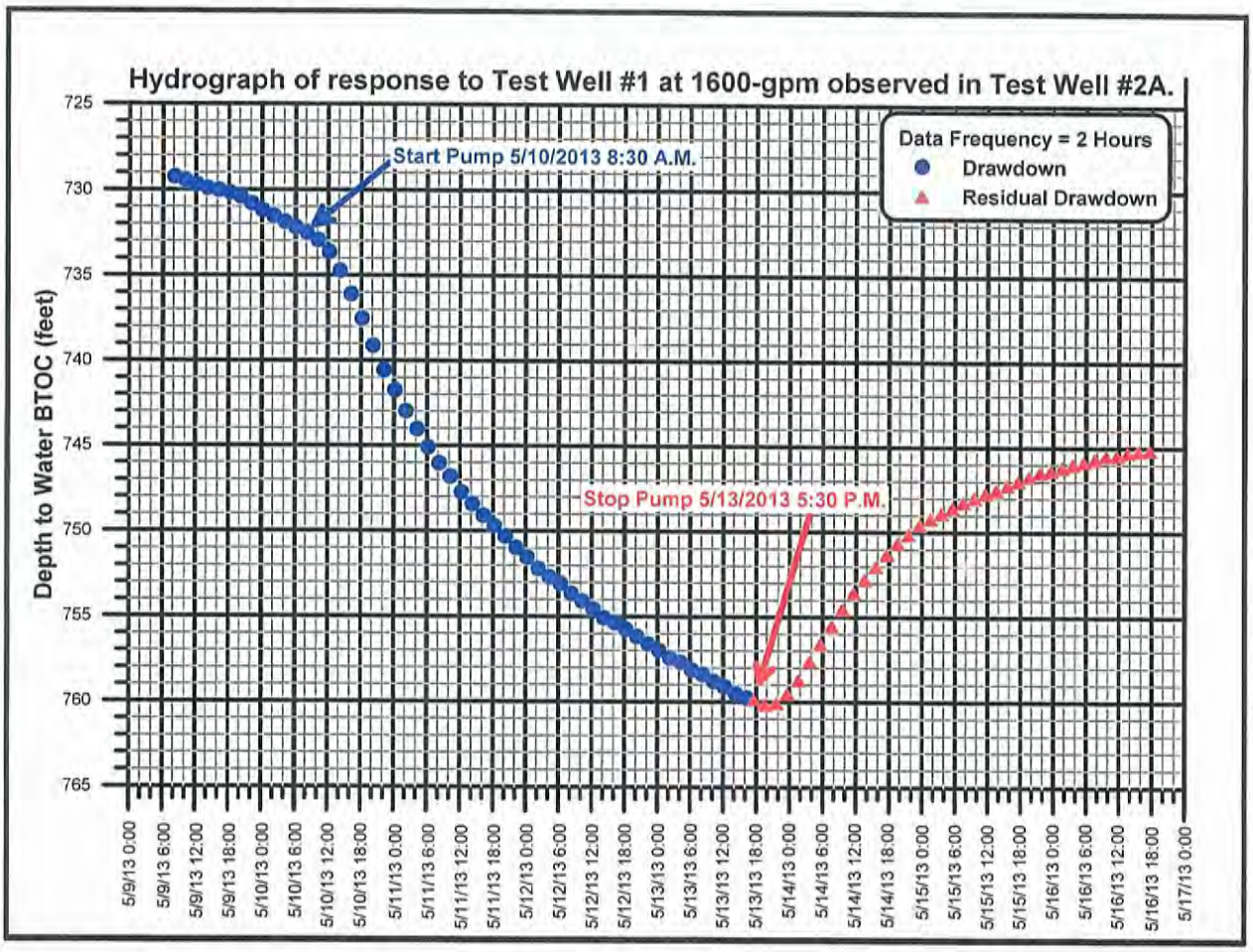

The residual drawdown record for Test Well #2A on Figure 41 ends at 5/16/2013, 5:36 P.M. with a depth to water of 745.128 feet BTOC. The depth to water at the corresponding time at Test Well #1 was 735.9 feet BTOC. Residual drawdown at Test Well #2A is 12.54 feet while that at Test Well #1 at the corresponding time (5:36 P.M.) is 7.15 feet. With the TOC elevation of Test Well #1 at 4571.8 feet and that at Test Well #2A at 4599.3 feet, the water surface elevation of 3854.2 in Test Well #2A is 18.3 feet higher than the water surface elevation of 3835.9 feet in Test Well #1.

This indicates that the recovery of the residual drawdown in Test Well #2A was being delayed until the cone of depression between the pumped well and the hypothesized high-conductivity fracture recovered to the elevation of the groundwater storage in the

fracture, so that flow out of the fracture was no longer necessary for recovery around the pumped well. At that time, all of the cone of depression would continue recovery at an accelerated rate, significantly greater than the projection of residual drawdown recovery on Figure 41.

5.5 Post-Frac Compared to Pre-Frac

Figure 42 shows post-frac drawdown and recovery at 1600 gpm compared to pre-frac drawdown and recovery at 900 gpm. The hydraulic improvement caused by acid stimulation is very evident in the comparison. The slope of the early pre-frac drawdown data is controlled by the aquifer transmissivity. However, the aquifer transmissivity should remain the same after acid stimulation of the well, except for the local area around the well that was affected by acid. Therefore, the slope of the post-frac data

Figure 42: Comparison of pre- and post-frac drawdown and recovery.

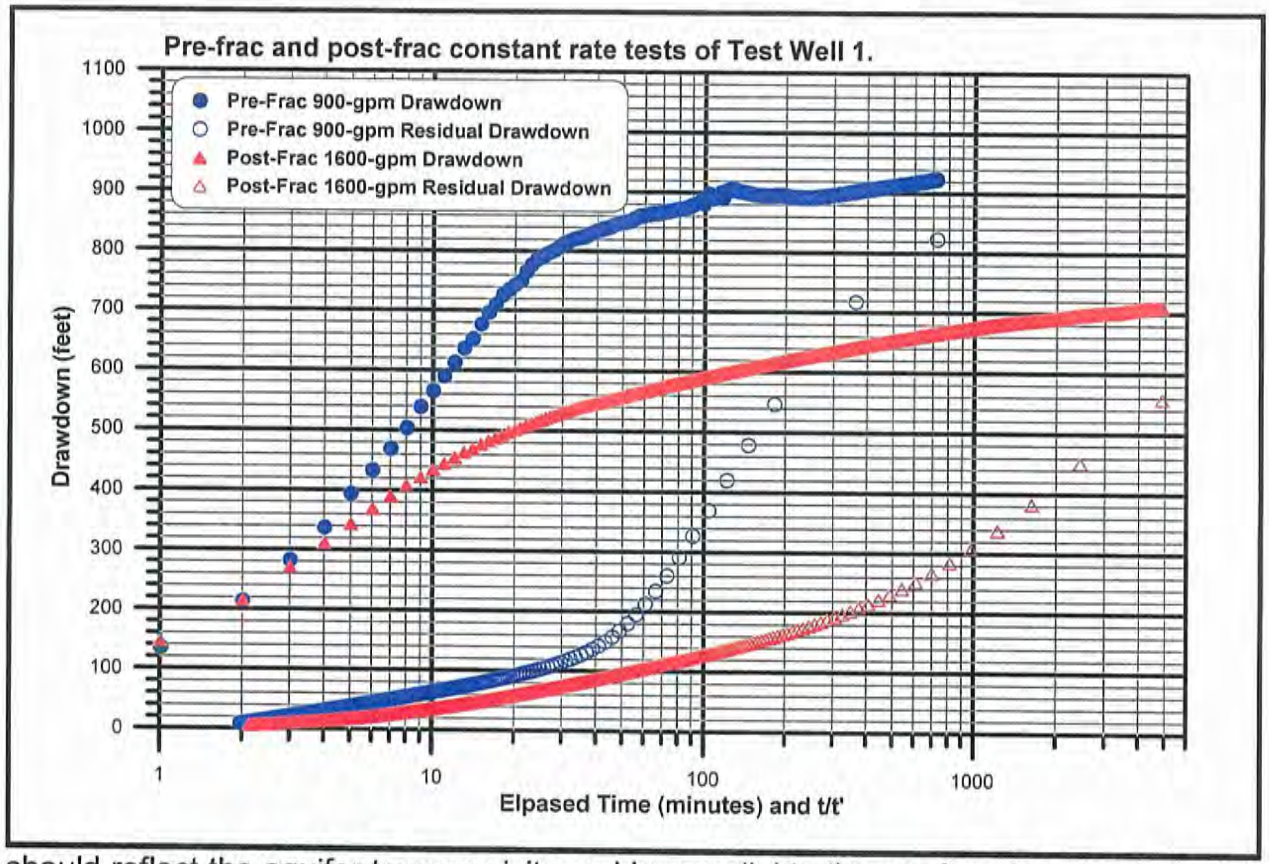

should reflect the aquifer transmssivity and be parallel to the pre-frac drawdown, even if post-frac drawdown is smaller; however, they are not parallel on Figure 42.

The significant departure of the post-frac data on Figure 42 from the slope of the early pre-frac data indicates that essentially all of the post frac drawdown and recovery was strongly influenced by recharge. This may indicate that during stimulation of the well, the acid followed a preferred path of least resistance, from the injection point in Test Well #1, to the hypothesized high-conductivity fracture, thus creating a situation where

post-frac pumping of the well immediately reacts to recharge from the high conductivity fracture.

5.6 Well Loss Drawdown

Figure 36 and the associated analysis provide the well loss coefficients, B and C, from the stepped test data. However, the well loss coefficients cannot be applied in a conventional manner to calculate well loss without caution. The equation for total drawdown in the well, s_w, is as follows:

$$S_w = BQ + CQ^2 \qquad \textbf{Equation 1}$$

where B = linear well loss coefficient
and C = nonlinear well loss coefficient

Equation 1 assumes that nonlinear well loss, CQ^2, is time dependent and predictable by conventional radial flow equations. Therefore, theoretical or "ideal" aquifer drawdown predicted by an equation such as the Theis equation can be subtracted from the total drawdown, s_w, and the difference is well loss drawdown. Equation 1 does not work in the case of the post-frac, 1600-gpm hydraulic performance of Test Well 31, because the ideal aquifer drawdown is not predictable by a conventional linear flow equation, due to the effects of recharge throughout the test response.

6 WATER QUALITY

Preliminary water quality samples were collected during air lift drilling of open hole through the Madison limestone and Whitewood dolomite strata. Figure 43 shows the concentrations of various chemical constituents plotted versus total depth of the advancing borehole at the time of sample collection. In general, all constituents increase somewhat in concentration as borehole depth increases. The plot includes the total dissolved solids concentration from a sample taken at the end of the 12-hour, 900-gpm constant rate, pre-frac aquifer test. Data for the plot are shown in Appendix E.

The data on Figure 43, and the analytical lab report in Appendix E for the pre-frac water quality sample collected during the 900-gpm constant rate test, provide the information about quality of water samples before the well was subjected to acid-frac stimulation.

Post-frac samples consist of iron and TDS data collected during the post-frac 1600-gpm yield and drawdown test and the analytical report for the final sample at the end of the 1600-gpm test. Iron and TDS information are shown with time-drawdown data on Figure 44. The TDS data are based on field measurements with an electrical conductivity meter set to provide TDS values based on the ratio between EC and TDS determined from previous laboratory analysis of water from the well. The final field measurement of TDS provided a value of 780.8 mg/L. A sample collected half an hour later and submitted to the laboratory for analysis had a TDS concentration of 817 mg/L, indicating the TDS meter readings included error due to the conversion factor or need